~~Measuring~~Field comparison of two novel open-path instruments that measure dry deposition and emission of ammonia using flux-gradient and eddy covariance methods ~~with two novel open-path instruments~~

Daan Swart[1], Jun Zhang[2], Shelley van der Graaf[1], Susanna Rutledge-Jonker[1*], Arjan Hensen[2], Stijn Berkhout[1], Pascal Wintjen[2,4], René van der Hoff[1], Marty Haaima[1], Arnoud Frumau[2], Pim van den Bulk[2], Ruben Schulte[1,3], Margreet van Zanten[1], Thomas van Goethem[1]

[1] National Institute for Public Health and the Environment (RIVM), P.O. Box 1, 3720 BA, Bilthoven, the Netherlands
[2] Netherlands Organisation for Applied Scientific Research (TNO), P.O. Box 15, 1755 ZG, Petten, the Netherlands
[3] Wageningen University & Research (WUR), P.O. Box 47, 6700 AA, Wageningen, the Netherlands
[4] Thünen Institute of Climate-Smart Agriculture, Bundesallee 68, 38116 Braunschweig, Germany

Correspondence to: susanna.jonker@rivm.nl

Abstract. Dry deposition of ammonia (NH_3) is the largest contributor to the nitrogen deposition from the atmosphere to soil and vegetation in the Netherlands, causing eutrophication and loss of biodiversity. Yet, data sets of NH_3 fluxes are sparse and in general have monthly resolution at best. An important reason for this is that measurement of the NH_3 flux under dry conditions is notoriously difficult. There is no technique that can be considered as the golden standard for these measurements, which complicates the testing of new techniques ~~and judging their quality.~~ . Here, we present the results of an intercomparison of two novel measurement setups aimed at measuring dry deposition of NH_3 at half-hourly resolution. In a five-week ~~comparison~~ period, we operated two novel optical open-path techniques side by side at the Ruisdael station in Cabauw, the Netherlands: the ~~novel~~ RIVM-miniDOAS 2.2D using the aerodynamic gradient technique, and the ~~novel~~ commercial Healthy Photon HT8700E using the eddy covariance technique. ~~Both are open-path optical~~These instruments~~, leaving NH_3 in the air during measurement. Otherwise, they~~ are widely different in their measurement principle and approach to derive deposition values from measured concentrations. ~~The two different~~ Yet, both techniques showed very similar results ~~when~~($r = 0.87$) and small differences in cumulative fluxes (~10%) as long as the upwind terrain was ~~both~~ homogeneous and free of nearby obstacles ~~($r = 0.87$).~~ The observed fluxes varied from ~~a deposition of ~~ -80 ~~ng NH_3 m^{-2} s^{-1}~~ to ~~an emission of ~~ +140 ng NH_3 m^{-2} s^{-1}. ~~We obtained similar results from two widely different techniques, both in~~ Both the absolute flux values ~~as in their~~and the temporal ~~pattern~~patterns were highly similar, which ~~substantiated~~substantiates that both instruments were able to measure NH_3 fluxes at high temporal resolution ~~for a consecutive period of at least several weeks.~~ However, for wind directions with ~~nearby~~ obstacles nearby, the correlations between the two techniques were weaker. ~~Moreover, the technical performance (e.g., uptime, precision) and practical limitations of both systems were discussed.~~ The uptime of the miniDOAS system reached 100% once operational, but regular intercalibration of the ~~two instruments~~system was applied in this campaign (35% of the 7-week uptime). Conversely, the HT8700E did not measure during, and shortly after, rain, and the coating of its mirrors tended to degrade (21% data loss during the 5-week uptime). In addition, the ~~HT8700E measured~~ NH_3 concentrations measured by the HT8700E proved sensitive to air temperature, causing substantial differences (range: -15 to + 6 µg m^{-3}) between the two systems. To conclude, the miniDOAS system ~~appeared~~appears ready for long-term hands-off monitoring. The current HT8700E system, on the other hand, had a limited stand-alone operational time under the prevailing weather conditions. However, under ~~the right circumstances~~relatively dry and low-dust conditions, the system can provide sound results, opening good prospects for future versions, also for monitoring applications. The new high temporal resolution data from these instruments can facilitate the

study of processes behind NH_3 dry deposition, allowing an improved understanding of these processes and better parametrization in chemical transport models.

1 Introduction

Human alteration of the global nitrogen cycle through agricultural, industrial, and combustion processes has led to unprecedented levels of reactive nitrogen (N_r) in the Earth system (Galloway et al., 2021; Fowler et al., 2013). Besides benefits like increased food production, losses of N_r have a range of detrimental effects on both the environment and human health (Sutton et al., 2011; Erisman et al., 2015). For example, many areas worldwide now experience increased levels of deposition of reduced nitrogen in the form of ammonia (NH_3) and ammonium (NH_4^+), which contribute to acidification and eutrophication of both terrestrial and aquatic ecosystems leading to the loss of biodiversity and ecosystem services . In addition, atmospheric NH_3, when transformed into NH_4^+, can form particulate matter in the atmosphere, which is increasingly recognised as a threat to human health .

. Gaseous NH_3 can be emitted from and deposited onto the Earth's surface: the exchange is bi-directional. NH_3 volatilisation during agricultural activities like manure and slurry storage and application, plus emissions from farm buildings, represent by far the largest source of anthropogenic NH_3 emissions . With regards to deposition, dry deposition of NH_3 is an important component. In the Netherlands for example, it typically accounts for more than a third of the total N_r deposition (Hoogerbrugge et al., 2020). The remainder is made up of dry deposition of oxidised forms of nitrogen, and wet deposition.. Accurate quantification of biosphere-atmosphere exchange of NH_3 is therefore essential to increase our understanding of NH_3 budgets at regional and global scales, to study relevant processes at high time resolution, monitor trends, measure the effectiveness of mitigation efforts, and improve and validate air quality and deposition models.

Despite the relevance of high-quality measurements of NH_3 exchange, relatively few direct long-term continuous measurements have been reported. Dry deposition of NH_3 can be highly variable in time and space and depends on a variety of site-specific parameters like canopy wetness, leaf area, and surface roughness (Flechard et al., 2011). Micro-meteorological techniques provide the most direct estimates of dry deposition, but these measurements each present their technical challenges and generally require substantial expense and labour. The most commonly used micrometeorological methods include the aerodynamic gradient method, modified Bowen ratio method, relaxed eddy accumulation, path-integrated techniques coupled with backward dispersion models, and eddy-covariance .

The aerodynamic flux gradient method (AGM, also 'profile method') has delivered the majority of the NH_3 dry deposition data worldwide. Most of these measurements were done using wet chemical instrumentation (e.g. Erisman and Wyers, 1993; Loubet et al., 2012), but nowadays also optical NH_3 measurement systems are used (e.g. Kamp et al., 2020). Wyers et al. describe the wet chemical denuder system that was used later in the Netherlands above forests and over heathland and in European intercomparison campaigns like the Braunschweig campaign . The AGM method is still commonly used for inferring half-hourly NH_3 fluxes, now also using optical NH_3 measurement systems .. In the AGM method, surface-atmosphere exchange fluxes are derived from measurements of vertical concentration differences (d_{NH_3}) combined with a measure of vertical turbulent transport (Loubet and Personne, 2016; Prueger and Kustas, 2005). Drawbacks of AGM (listed by Trebs et al., 2021; Loubet et al., 2013) include potentially biased gradients under non-stationary conditions if sequential sampling at multiple heights using one monitor is required (Kamp et al., 2020), or, if using multiple monitors, the need for regular side-by-side comparisons to accurately determine and correct for any potential systematic difference (bias) between monitors (Wolff et al., 2010; Walker et al., 2013). Because of its reactivity and solubility in water, NH_3 is sticking to inlet walls, filters and measurement cells . Systems with an inlet system, either wet chemical or optical with a closed sampling cell, will be prone to sampling carry-over NH_3 due to NH_3 being adsorbed and released again inside the measurement system. This is affecting the measured concentration gradient and thus the fluxes derived with the AGM technique.. Finally, a drawback of AGM is the

need to rely on empirical stability corrections, which are based on relationships found for sensible heat, but assumed to be the same for trace compounds like NH_3.

Open-path (OP) techniques avoids the delay effects, reduced temporal resolution and interference from aerosols that result from NH_3 sticking to inlet lines, air filters and other surfaces in an instrument (Parrish and Fehsenfeld, 2000)~~Open-path (OP).~~ OP analysers have no sampling tubes and provide a way of measuring concentration in situ, without interfering with the airflow. A long-line averaging open-path gas analyser allows measurements of path integrated NH_3 concentrations at a high time resolution. Optical analysers now available include those based on Fourier Transform Infrared (FTIR) (Sintermann et al., 2011; Flesch et al., 2016), tuneable diode laser TDL (Bai et al., 2022) or differential optical absorption DOAS spectroscopy (Volten et al., 2012b; Sintermann et al., 2016). These instruments can be used to measure the difference in NH_3 concentration between two vertically offset paths, either in slant configuration (e.g. Bai et al., 2021; Flesch et al., 2016) or in two parallel horizontal paths. In the Netherlands, several experiments have taken place using two DOAS systems to measure d_{NH_3} (Wichink Kruit et al., 2010; Volten et al., 2012a; Schulte et al., 2020). Over the last year, the more recently developed miniDOAS (Berkhout et al., 2017) has been adapted and improved to meet the high sensitivity required for flux gradient measurements of NH_3 (Wolff et al., ~~2010a~~2010; Foken, 2017).

Eddy covariance (EC) is the preferable technique for measuring the surface-atmosphere gas exchange of any compound because it provides the most direct measurement. ~~For many greenhouse gases, it has already become the reference method .~~ However, EC requires fast (<0.1 s) and precise concentration measurements, which is particularly challenging for NH_3. In recent years, several studies have reported measurements of the NH_3 flux using closed-path (CP) analysers (Famulari et al., 2004; Moravek et al., 2019; Zöll et al., 2016)~~based on different techniques like a tandem mass spectrometer , high-temperature chemical ionization mass spectrometry , and laser-based solutions like the tuneable infrared diode laser differential absorption spectroscopy (TILDAS) technique or a quantum cascade laser (QCL) instrument . However, the 'stickiness' mentioned above.~~ However, the reactivity and solubility of NH_3 in water presents challenges there, because the use of inlet tubing leads to loss of fast variations in the signal. ~~The amount of damping of the signal is highly variable, and depends on temperature, humidity, and cleanliness of the tubing, among other things. Correcting for this high-frequency loss introduces additional uncertainty .~~

So far, two folded-path open-path instruments ~~have been reported in the literature~~are available for eddy covariance measurements of NH_3. Besides the benefit compared to the CP setup of not needing an inlet tube, such systems generally have much lower power requirements and the less bulky installation may allow for a more portable and adaptable setup also at more remote sites.

The first OP EC NH_3 analyser is the QCL-based instrument developed by Princeton University, and improved from the original design presented in Miller et al. (2014) over various deployments (Sun et al., 2015; Pan et al., 2021). More recently, a similar instrument has become available from Healthy Photon Co. Ltd., Ningbo, China: model HT8700 (Wang et al., 2021). Limitations of open-path EC flux measurements include interference from contamination by dust and rainfall, and ~~degradation of mirrors over time .~~the influence of exposure of the instrument to outdoor conditions. Since this technique is evaluating the net flux by measuring concentration levels in both up and down going air that passes the sensing volume both in small, high frequency (> 5 Hz) eddies and in slow (> 10 minute) large turbulent eddies the method needs corrections for differences in air density between up and down going air ~~linked with heat and humidity transport.~~ Similar to closed-path EC gas analysers, not all sizes and frequencies of eddies are measured completely and therefore (high and low frequency) spectral corrections are needed.

Both micrometeorological methods (AGM and EC) share additional limitations to those mentioned above, such as the need for a homogeneous upwind fetch to avoid local advection errors. They also require steady-state conditions, well-developed turbulence, with no change in vertical flux with height (Loubet et al., 2013; Mauder et al., 2021).

In this study, we measured bi-directional NH_3 fluxes in a field campaign of seven weeks from August 24th to October 11th, 2021 over grassland at the Cabauw research site in the Netherlands, during which both deposition and emission events were

encountered. During a period of 5 -weeks (August 27th to October 1st), we compared measurements of NH_3 concentrations and fluxes from two open-path instruments: the RIVM miniDOAS 2.2D using the AGM, and the commercial HT8700E from Healthy Photon Inc. using the EC technique. This was the first time either one of these systems was compared to another setup. The primary aim of the campaign was to test if both novel instruments were indeed capable of measuring the dry exchange flux of NH_3 at high temporal resolution. Here, we describe the uptime and performance of both setups and compared the results of both concentration and flux measurements of NH_3. Moreover, potential sources of errors, challenges encountered and the current suitability and future potential of the different setups for long-term in-situ measurement under field conditions are discussed.

2 Campaign setup and site

2.1 Site description

NH_3 measurements were performed at the Cabauw site for atmospheric research (51.97034° N, 4.92559° E, elevation –0.7 m a.s.l.). The site is operated by Royal Netherlands Meteorological Institute (KNMI) and has been an atmospheric research station for over half a century (Bosveld et al., 2020). It hosts an extensive suite of meteorological and atmospheric instrumentation, some on the 213 m high mast on the facility. It is also one of the stations of the Dutch National Air Quality Monitoring Network and since 2019 part of the Ruisdael observatory (https://ruisdael-observatory.nl/the-rita-2021-campaign/, last access date: 20 Apr 2022). The site is 15 and 25 km away from the urban areas of Utrecht and Rotterdam, respectively (Figure S1). The area is completely flat (slopes less than 3%), with ribbon-shaped villages built along minor watercourses. Land use in the general area is predominantly agricultural, with most plots intensively managed grassland with an average vegetation height of 0.1 m used to graze cattle or sheep, or for silage. The soil consists of 35-50% river clay in the top 0.6 m, overlying a thick layer of peat (Bosveld, 2020). The soil of the top layer (0–0.15 m) has a bulk density of 1.14 g cm^{-3} (Jager et al., 1976). The measurement site is drained by narrow (1-3 m) parallel ditches, which are on average 40 m apart. ~~The site policy is to keep the grass short by having it grazed by sheep.~~

To illustrate the distribution of the different land cover classes within the footprint of the instruments, an unsupervised land use classification is provided in Figure S2 of the supplementary materials. Moreover, Figure S3 illustrates the differences in management of individual paddocks in the flux footprint through time. During the campaign, sheep were grazing the plots of land immediately surrounding the measurement site. To prevent sheep from blocking the miniDOAS optical paths or from damaging instrument cables, the measurement area was secured with a low profile electric fence. ~~During the campaign, sheep were grazing the plots of land immediately surrounding the measurement site.~~ These sheep often grazed within 100 m north to northeast of the instruments with about 50 animals per hectare. Furthermore, the plots surrounding the research site were occasionally manured by local farmers, which was allowed up until September 15~~ (RVO, https://www.rvo.nl/onderwerpen/mest/gebruiken-en-uitrijden/wanneer-uitrijden, last access 12 May 2022).~~ .

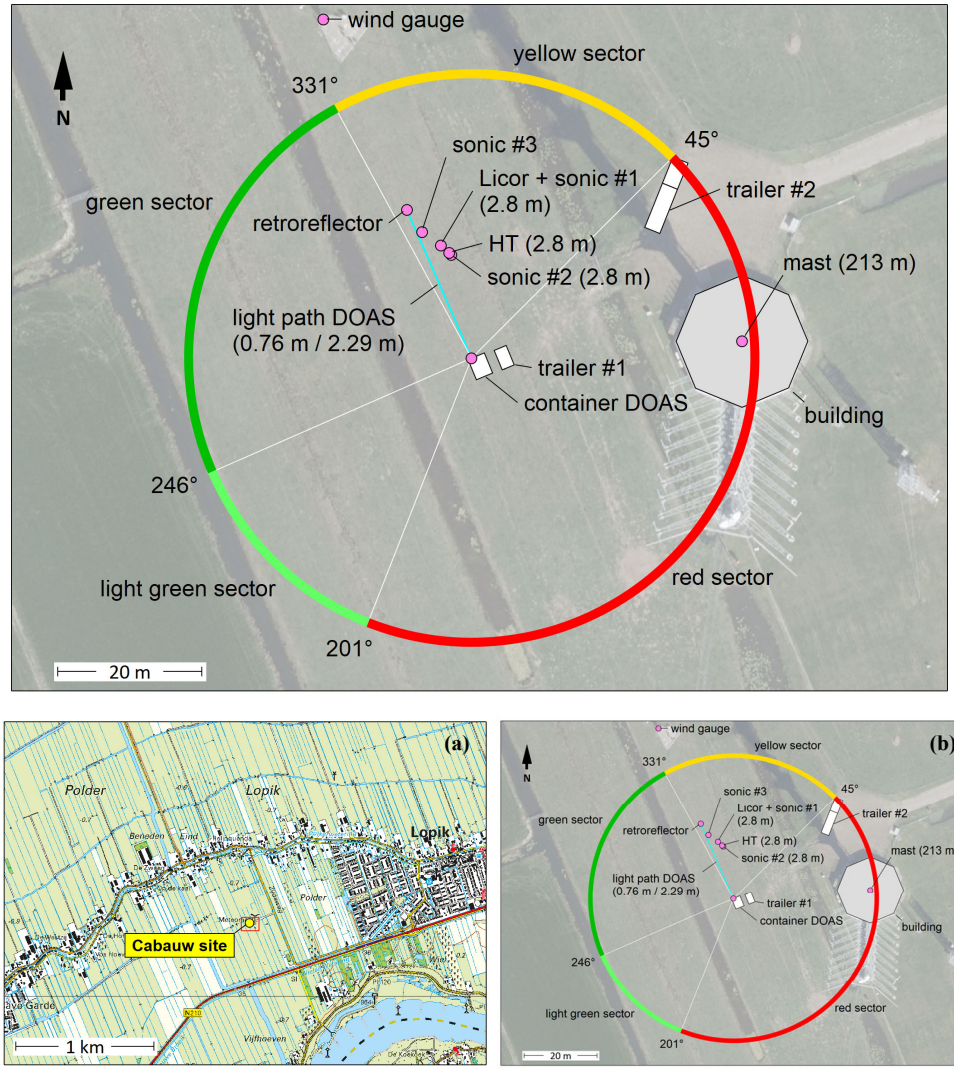

Figure 1. The area surrounding the Cabauw measurement site (a). Cabauw is in a flat area at -1m, being in the delta of the river Lek shown in the south east. The line with housing going east-west, running north of the tower has a series of farms. Map from www.pdok.nl/~~the location~~ (downloaded 07-02-2021). The locations of the instruments. (b). The coloured circle denotes wind origin sectors which are used for filtering data (see text). The green and light-green sectors indicate wind directions with minimally obstructed flow. Wind from the yellow sector is somewhat obstructed. Wind from the red sector experiences severe obstruction due to the building at the foot of the tall mast, the trailers and the DOAS container. Background aerial photo from opendata.beeldmateriaal.nl (downloaded 22-02-2022). Data of sonic #3 is not used in the final analysis.

2.2 Instruments overview

For this campaign, the following instruments were set up in a field next to the 213 m mast at Cabauw. The two miniDOAS NH_3 instruments were placed above each other in a small container (see below for a detailed description of these instruments). The 22.1 m optical paths were directed at 336°, parallel to the ditches between the fields. The bottom path was at 0.76 m and the top path 2.29 m above the field. Anticipating prevailing winds from the south-west, the other instruments were positioned 3 m east of the miniDOAS optical paths (Figure 1), to minimise distortion of the incoming airflow. The instruments each

integrated spectra during 4 minutes and provided simultaneous path-averaged concentration values at 4-minute intervals. These concentrations were then averaged to 30-minute values. The HT8700E open-path NH_3 analyser (see below for a detailed description of this instrument; hereafter referred to as 'HT'), was mounted on a steel mast with the centre of its optical path at 2.80 m above the ground. On a second steel mast, 1.5 m from the first, a sonic anemometer (sonic #1; model Gill WindMasterPro™, Gill Instruments, Lymington, UK) was mounted. This sonic measured the 3D wind components at 32 Hz 2.8 m above the ground. The 10 Hz open-path H_2O and CO_2 analyser (LI-7500DS, LI-COR Biosciences, Lincoln, USA) was placed at 2.83 m above the ground next to sonic #1.

From September 30 onwards, to evaluate the impact or sensor separation between the HT and the sonic #1 on the calculated NH_3 fluxes, a second sonic anemometer (sonic #2, model Gill WindMaster™, Gill Instruments, Lymington, UK) measuring at 32 Hz was installed 40 cm from the HT analyser. ~~A third sonic, #3, was placed from the beginning of the campaign along the path but its data were not used in the final analysis. Because its presence may still influence the wind across the DOAS path it is included in .~~

~~Data storage, power supplies, and remote control apparatus for these instruments were housed partly in the DOAS container and partly in trailer #1 parked next to this container. During part of the campaign, a large trailer#2 with additional instruments was parked to the north-north-west of the 213 m mast.~~

In Figure 1 we show different coloured wind sectors. The selection is based on objects on the site that influenced the wind field and thus the flux intercomparison. The four wind sectors (Figure 1) were:

a) The green sector (246°–331°): minimal disruption. Only the drainage ditches are expected to influence the wind field.
b) The light green sector (201°–246°): minimal disruption. We expected the DOAS container to have some influence.
c) The yellow sector (331°–45°): some disruption. The masts with HT and the sonics disturbed the wind field at the DOAS paths. At times, the sheep farmer positioned a small trailer there on the field to the north of the 213 m mast, and sheep were grazing there. This would have affected all instruments.
d) The red sector (45°–201°): severe disruption. The 213 m mast, the building at the foot of this mast, the trailers and the DOAS container all affected all instruments.

Figure 2. The instruments, seen from the miniDOAS container looking north. From left to right: 10 m wind vane mast, mast with the two retroreflectors of the miniDOAS instruments, mast with sonic #3, mast with sonic #1 and LI-7500DS; mast with HT8700E and its cooling unit. Sonic#2 was placed later at 40 cm on the southeast side of HT8700E on the same mast (not shown in the photo). The 213 m mast is off to the right (east).

2.3 Weather conditions

~~The Cabauw site has a mean annual air temperature of 10.4 °C and a mean annual precipitation of 770 mm. The thirty-year average temperature for September is 14.8°C, and the total precipitation is about 84 mm (KNMI, https://www.knmi.nl/klimaat-viewer, last access 12 May 2022).~~ Historically, winds from the southwest tend to be most common in September. During the campaign, the weather was slightly warmer and substantially drier than normal for this time of year (Homan, 2021) (Figure ~~S2~~S4). However, there were no ~~extreme~~extremely hot or cold spells. No significant precipitation occurred during the measurement period, except for a few short shower events late September. The wind direction during the campaign was variable and therefore different from the expected predominant wind direction.

3 Methods

3.1 Aerodynamic gradient method (AGM) NH_3 fluxes

3.1.1 MiniDOAS instruments

DOAS, short for differential optical absorption spectroscopy, is an optical technique to measure trace gas concentrations over an open path in the atmosphere (e.g. Platt and Stutz, 2008). ~~An open-path technique avoids the delay effects, reduced temporal resolution and interference from aerosols that result from NH_3 sticking to inlet lines, air filters and other surfaces in an instrument . These qualities are especially relevant for NH_3 measurements in open air.~~

For this experiment, two identical RIVM miniDOAS 2.2D instruments were used. These are active DOAS systems, i.e., equipped with their own light source rather than using sunlight. The light is sent to a retroreflector over an open path of 22.1 meters and received back (Figure 3). Path-averaged NH_3 concentrations are retrieved from spectra taken in the 200–230 nm wavelength range.

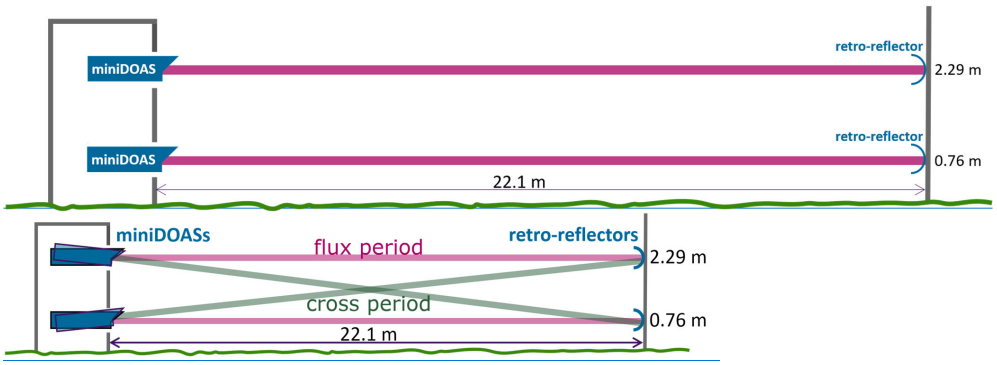

Figure 3. MiniDOAS setup in the field, using two instruments at different heights above the ground. The NH_3 flux is determined from the observed concentration difference between top and bottom paths and the turbulence measurements of sonic~~#1.~~ #1 (flux period, shown in purple). Shown in green are the two instruments in cross-position (cross period). These zero-difference measurements are used for the precise intercalibration needed for flux measurements (see text).

The 2.2D instruments are a modified and further developed version of the miniDOAS 1.x described earlier (Berkhout et al., 2017; Volten et al., 2012b). MiniDOAS 1.x instruments have been operating in the Dutch national air quality monitoring network ~~(LML, Landelijk Meetnet Luchtkwaliteit, https://www.luchtmeetnet.nl/, last access date: 20 Apr 2022)~~ since 2016~~, providing hourly concentration measurements of NH_3 concentrations in ambient air~~ at six locations ~~in the Netherlands.~~. The uptime of these instruments in 2021 was above 95% of the hourly values.

Improvements in the 2.2D version include the use of a more sensitive charge-coupled device detector and several optical components with higher reflectivity and/or transmission in the wavelength range used, leading to about a factor of 5 increase in optical throughput. The optical layout was simplified and an optical scanner was added, making the system less sensitive to small alignment changes. These modifications resulted in a substantial increase in precision and stability of the measurements, as was needed for the monitoring of dry NH_3 fluxes with the AGM method. We aim to describe the miniDOAS 2.x in more detail in a forthcoming publication, in combination with the implementation of this version in the Dutch national air quality monitoring network LML.

~~For the AGM measurement, two miniDOAS 2.2D instruments were installed in an air-conditioned container and placed on a stable metal frame attached to the container wall. Optical paths through quartz windows were located at 0.76 m and 2.29 m height, parallel to the local soil surface. The instruments each integrated spectra during 4 minutes and provided simultaneous path-averaged concentration values at 4-minute intervals. These concentrations were then averaged to 30-minute values.~~

3.1.2 MiniDOAS calibration and intercalibration

As the AGM method depends on the ability to measure small concentration differences between two heights, great care must be taken to calibrate the two miniDOAS instruments properly, first individually and then as a pair, and to maintain this calibration over the flux measurement period. This process is described below.

3.1.2.1 Initial individual lab calibration

~~After assembly or maintenance, the individual miniDOAS instruments were~~Each instrument was calibrated according to the procedures used in the LML-network. This included the acquisition of a 'reference spectrum' with known, preferably zero, concentrations of NH_3, ~~nitrogen oxide,~~SO_2 and ~~sulphur dioxide~~NO. For this, the zero-tunnel calibration facility at RIVM was used. This spectrum served as a common reference for all measurements. We also acquired 'calibration spectra' of the three gases mentioned, using a flow cell in the light path in combination with the zero-tunnel facility. These spectra contain the

spectral fingerprint and cross-section of these gases, used in the analysis. For this step, calibration gases of these components with a supplier-indicated accuracy of 2% were used.

Afterwards, the accuracy of the NH_3 calibration was tested by providing two NH_3 mixtures in ~~nitrogen~~N_2 from certified reference cylinders, representing a low and a high concentration of about ~~30 mg~~35 µg m^{-3} and ~~300 mg~~350 µg m^{-3} in the atmosphere, respectively (Certified Reference Materials, produced by the Dutch metrological institute VSL). These reference cylinders have a certified accuracy of 3% and 2% respectively. The instrument calibration was considered valid if the measurement result was within 3% of the certified reference.

3.1.2.2 Additional intercalibration for deposition

While suited for concentration monitoring, the calibration approach above is not precise enough for AGM, where concentration differences of 0.1 µg m^{-3} or better need to be determined, i.e., well below the 1% level. For this, an additional calibration of the two miniDOAS instruments is needed, as a pair. This was done after installation in the field.

The instruments were manually set to a different alignment position, as indicated in Figure 3, the so-called cross-position. ~~To achieve this, a miniDOAS instrument pivots as one piece on a ball joint located near the quartz windows.~~ As both instruments now sample on average the same height region, results should be identical for all flow situations where the NH_3 gradient is homogeneous over the horizontal path. In this cross-setting, the instruments were set to run for several days, until a sufficient amount of variation in outside air concentrations were encountered. Typically, the intercalibration lasts at least 3 days under ~~ideal weather conditions (wind from an unobstructed direction, sufficient turbulent mixing).~~suitable conditions.

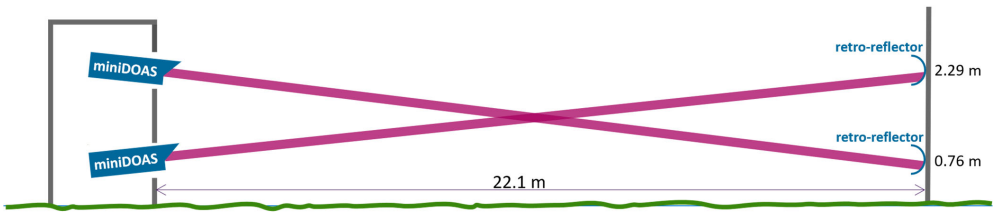

~~**Figure . MiniDOAS setup in the field, using two instruments in the cross-position. These zero-difference measurements are used for the very precise intercalibration needed for flux measurements (see text).**~~

First, new simultaneous reference spectra for both instruments were obtained from the dataset obtained during the intercalibration, to replace the reference spectra obtained in the zero-tunnel. The obtained absolute concentration values from these spectra will be less accurate, i.e., they may have a small but fixed offset to the lab. They will however be more precise. ~~This~~ which is ~~a useful step, as~~essential for ~~the flux measurement the concentration difference between the two systems needs to be determined with minimum random error.~~gradient measurements. Next, the spectra obtained in the cross period were processed with these new reference spectra.

When comparing the results from both instruments in a ~~scatterplot~~scatter plot, the minor additional corrections to the offset and span can be obtained that are needed to make the instruments match perfectly, with offset 0 and slope 1.

In the Results section (Sect. 4.1), it will be illustrated that after these steps the pair was capable of measuring NH_3 differences ~~well below~~within our target precision of 0.1 µg m^{-3}. The new field reference spectra and the small additional corrections obtained in the cross-position are kept and also applied in the analysis of the flux measurements obtained in the parallel position.

3.1.3 Flux calculation

The 30-minute concentration measurements obtained at the two measurement heights were combined with 30-minute averaged transfer velocities to obtain the AGM NH_3 flux F_{AGM}, (e.g. Trebs et al., 2021):

Field Code Changed

$$F_{\mathrm{AGM}} = -\frac{ku_*}{\ln\left(\frac{z_2}{z_1}\right) - \Psi_{\mathrm{H}}\left(\frac{z_2}{L}\right) + \Psi_{\mathrm{H}}\left(\frac{z_1}{L}\right)} \times [c_{\mathrm{NH_3}}(z_2) - c_{\mathrm{NH_3}}(z_1)] \qquad \text{Eq. 1}$$

Where u_* is the friction velocity; k is Von Kármán constant (0.4), $c_{\mathrm{NH_3}}(z_n)$ is the NH_3 concentration at height z_n ~~and;~~ z_1 and z_2 are the heights of the bottom and top miniDOAS paths above the displacement height d (assumed 2/3 of the canopy height), respectively. $\Psi_{\mathrm{H}}\left(\frac{z}{L}\right)$ is the integrated stability function for heat, which is assumed to be the same for NH_3. L is the Monin-Obukhov length. For unstable conditions ($L < 0$), we used the functions of Dyer (1974) and Paulson (1970). For stable conditions ($L > 0$), we used the function of Beljaars and Holtslag (1991). Micrometeorological parameters u_* and L were calculated using EddyPro software version 7.0.6 (LI-COR Biosciences, Lincoln, USA) using data collected ~~using~~by sonic #1. AGM fluxes were calculated using custom software written in R. We follow the sign convention where positive fluxes indicate emissions and negative fluxes deposition.

3.2 Eddy covariance (EC) NH_3 fluxes

3.2.1 HT8700E instrument

The open-path QCL-based NH_3 analyser (Healthy Photon Lt. Co., Ningbo, China, Model HT8700E; hereafter HT) was used to measure NH_3 concentrations at 10 Hz using the wavelength modulation spectroscopy technique. Technical details of the analyser have been described in Wang et al. (2021). The QCL sends a beam at 9.06 µm into an open-air Herriott cell which has two concave mirrors of high purity molybdenum with a coating that should withstand frequent cleaning with organic detergents. The temperature of the QCL and detectors are stabilized by Peltier thermo-electrical coolers (TEC). The analyser is coupled to a compact external water and ethylene glycol chiller (Wang et al., 2021).

The HT8700 performance in laboratory and field experiments ~~have~~has been presented by Wang et al. (2021, 2022). The uncertainty of the NH_3 concentration measurements was estimated to be ±15% by comparing two commercially available high-sensitivity NH_3 analysers G2103 (Picarro Inc., Sunnyvale, USA) and EAA-911 (Los Gatos Research (LGR), San Jose, USA) in the lab (Wang et al., 2021). ~~Instrumental noise was first reported as 0.30 ± 0.046 ppbv after a one-week deployment in a subtropical rice paddy field in Southern China, with a flux detection limit of 7.1 ± 1.1 µg N m^{-2} h^{-1} (equivalent to 2.4 ± 0.4 ng NH_3 m^{-2} s^{-1}).~~ In the follow-up study (Wang et al., 2022), a slightly higher noise ratio (0.41 ± 0.06 ppbv) and flux detection limit (9.6 ± 1.5 µg N m^{-2} h^{-1}, equivalent to 3.2 ± 0.5 ng NH_3 m^{-2} s^{-1}) were found after one-month long monitoring at a wheat field in Northern China. ~~The HT was calibrated in the factory using a glass tube that enclosed the open optical cell. Zero calibration was done by flushing the cell with pure nitrogen. For span calibration, a NH_3 permeation tube and dilution system (KIN-TEK Analytical, Inc., La Marque, USA) was used. The permeation tube released a fixed rate of NH_3 at stabilized temperature. Different NH_3 concentrations in N_2 were provided with the diluter to the cell inserted into the instrument. The off-factory calibration points of our instrument had rather larger values (0 – 450 µg m^{-3}) than typical field concentrations at the Cabauw site, but good linearity was obtained throughout the lab calibration range according to the manufacturer.~~

Raindrops, dust, and other contaminants on the mirrors (particularly the bottom one), cause light scattering which is shown in the optical signal strength (OSS) of the HT (Wang et al., 2021). In contrast to Wang et al. (2021, 2022) in this experiment we used an upgraded HT version being equipped with an automated mirror cleaning system (the SPIDER®) that can be activated remotely, which significantly reduced the manual cleaning burden. During this campaign whenever the OSS value dropped below 40% the lower mirror was cleaned using the SPIDER® ~~that was activated remotely~~ for 1 to 2 minutes at a time. In

addition, both mirrors were manually cleaned 1-2 times per week using lens tissue drenched in methanol if automatic cleaning was not sufficient. However, the OSS values gradually decreased over the experimental period especially after multiple rain events before the end of the campaign (Figure ~~S3~~S5).

3.2.2 Flux calculation

The EC NH_3 fluxes and other micrometeorological parameters were calculated using EddyPro software (version 7.0.6, LI-COR Biosciences, Lincoln, USA) at 30-minute intervals using the 10 Hz 'raw' data. The general flux calculation procedure followed the standard FluxNet methodology (Mcdermitt et al., 2011) and some basic settings are following Wang et al. (2021). For detailed settings and parameters of this study see Table S1. In addition to the analysis in EddyPro, additional spectral analyses were further tested to study the impact of high-frequency spectral damping and sensor separation on the flux results.

3.2.2.1 High frequency spectral losses correction

The eddy flux method evaluates the vertical transport of gas, heat or momentum caused by a composition of turbulent eddies that cover the spectrum from cm to km scale or, in the time domain, from 10 Hz to 30 min scale. Measured EC fluxes correlate the vertical wind and the concentration variation, the covariance which can be visualised in a cospectrum showing the contribution of the large and small turbulent motions. The raw measurement data need corrections for turbulence-spectral losses both in the low (> minutes) and high (> 1 Hz) -frequency range. For the open-path system, the former is caused by the finite averaging time, as the measurement system will not "see" large scale eddies that take longer than the 30-minute evaluation interval. The concentration changes that occur with a high frequency (linked to small eddies) are ~~damped~~dampened due to the sensing volume of the instrument (which is 50 cm high and will not show eddies that are 10 or 5 cm in diameter) and due to the spatial separation between sonic anemometer and gas analyser (Moore, 1986).

Using the EddyPro software, low-frequency flux losses were corrected according to Moncrieff et al. (2004). For estimating high-frequency flux losses ~~for the open-path analyser, the theorical~~, the theoretical method from EddyPro (hereafter referred to as TEO; Moncrieff et al., 1997) was applied first. Two remarks have been made on this procedure. First, a difference can occur between the measured cospectra and the theoretical frequency distribution of Kaimal cospectra (Kaimal et al., 1972; Moncrieff et al., 1997). Second, in EddyPro's implementation of Moncrieff et al. (1997) the correction for sensor separation is independent of the wind direction, which holds as long as the distance between the sonic anemometer and gas analyser is relatively small (Moore, 1986). Moore (1986) already indicated that in doing so the flux correction would probably be overestimated. Therefore, to better understand the real field condition and equipment separation results in EC flux, an empirical approach using measured gas flux cospectra and sensible heat cospectra as reference was applied similar to Wintjen et al. (2020, hereafter referred to as ICO after 'in situ cospectral method')). ~~In short, a cospectrum shows how much each frequency (eddy) contributes to the flux. A fitting of the normalised temperature based on the trace gas cospectra using an empirical transfer function shows how well the gas analysers can resolve the contribution of eddies in the high-frequency range of the gas flux cospectra and therewith suffer from damping effects that are assumed to be absent for temperature. We used the same empirical transfer function as Wintjen et al. and made the non-linear fit for frequencies higher than 0.1 Hz. For further details on the cospectral correction method, we refer to Sect. 2.3.2 of Wintjen et al. . To ensure the quality of the half-hourly damping correction factors, values were filtered according to the following criteria: QC flag 0 in Eddy Pro ; u_* > 0.1 m s^{-1}; the variances in the NH_3 concentration are below 2 times the standard deviation plus the mean of the overall campaign period; EddyPro found a maximum in the covariance within the prescribed time lag window. In total, 661 half-hour NH_3 correction factors were left for correcting their respective fluxes. If half-hourly corrections factors were not available due to quality criteria, we used daily medians to correct corresponding fluxes.~~For detailed ICO method data quality control, see Sect. 1.1 in the supporting materials.

3.2.2.2 Modified WPL correction

Open-path trace gas concentrations are affected by density variations in the up- and down going air movements. The Webb-Pearman & Leuning (WPL) correction accounts for that (Webb et al., 1980). Two WPL methods were used. First, the classic WPL method was used to correct H_2O measurements from LI-7500DS. Part from that, the NH_3 flux is also affected by spectroscopic effects (Burba et al., 2019). The spectroscopic part is instrument dependent and deals with the effect of changing H_2O concentrations and their impact on the absorption line used for NH_3. Hence, the modified WPL method was applied to correct the HT-measured NH_3 flux following Wang et al. (2021):

$$F_{\mathrm{EC}} = A\left[\overline{w'\rho_{\mathrm{A}}'} + B\mu\frac{\overline{\rho_{\mathrm{A}}}}{\overline{\rho_{\mathrm{d}}}}\overline{w'\rho_{\mathrm{v}}'} + C\left(1+\mu\frac{\overline{\rho_{\mathrm{v}}}}{\overline{\rho_{\mathrm{d}}}}\right)\frac{\overline{\rho_{A}}}{\overline{T_{\mathrm{a}}}}\overline{w'T_{\mathrm{a}}'}\right] \qquad \text{Eq. 2}$$

where ρ_{A} is the NH_3 density corrected for temperature (see Sect. 4.1.2), ρ_d is the dry air density, ρ_{v} is the water vapor density, μ is the molar mass ratio of dry air to water vapour, $\overline{w'\rho_v'}$ is the water vapour flux measured by the LI-7500DS, T_{a} is the air temperature and $\overline{w'T_a'}$ is the sensible heat flux from the sonic anemometer. A, B, and C are dimensionless parameters accounting for the spectroscopic effects from (Wang et al., 2021)., which vary with ambient temperature, pressure and water vapour content.

3.3 Quality control and filtering

~~The quality control of the AGM and EC NH_3 fluxes was proceeded as follows.~~Firstly, observations from the HT were filtered out before the EC flux analysis if the optical signal strength (OSS) of the NH_3 analyser was below 40% (Figure ~~S3). Firstly~~S5). Secondly, after EC analysis in EddyPro was completed, EC fluxes were removed if a quality flag of 2 was assigned according to the stationarity and integral turbulence tests proposed by Mauder and Foken (2006). ~~Secondly~~Thirdly, both ~~the EC and AGM~~ fluxes with u_* values smaller than 0.1 m s^{-1} were discarded, to filter out observations during low-turbulent mixing conditions. ~~Thirdly~~Fourthly, a moving window outlier filter was applied to the remaining ~~EC and AGM~~ fluxes, removing points if two times the standard deviation of the adjacent six flux values was exceeded (Wang et al., 2021; Wang et al., 2022). Finally, the data was grouped into 4 different wind sectors (green, light green, yellow and red) as described in Figure 1. Only observations from the green and light green sectors were used for the intercomparison of the ~~AGM and EC~~ fluxes. An overview of the applied filters and the percentage of accepted fluxes per filter step are shown in Table S2 in the supplementary materials.

3.4 Uncertainty analysis

~~(~~A description of the random error analysis of the half-hourly AGM ~~NH_3~~and EC fluxes ~~($\sigma_{F_{AGM}}$) from the miniDOAS instruments has three error components and was estimated as follows:~~

~~Here, the three error components are:~~

~~1. the relative error of the u_* values, $\frac{\sigma_{u_*}}{u_*}$,~~

~~2. the relative error of the difference~~is given in ~~the miniDOAS NH_3 concentration at height z_1 and z_2, $\frac{\sigma_{c_{NH_3}(z_2)-c_{NH_3}(z_1)}}{c_{NH_3}(z_2)-c_{NH_3}(z_1)}$,~~

~~3. and an error term related to the stability correction at each measurement height, $\frac{\sigma_{f(z,\Psi)}}{f(z,\Psi)}$, with~~

~~$f(z,\Psi) = \ln\left(\frac{z_2}{z_1}\right) - \Psi_H\left(\frac{z_2}{L}\right) + \Psi_H\left(\frac{z_1}{L}\right)$.~~

~~The relative errors of the u_* are estimated in EddyPro following Finkelstein and Sims . The relative error of the miniDOAS NH_3 concentration differences is determined to be 0.088 µg m^{-3} during the cross periods (see~~ Sect. ~~). Finally, we assumed that~~

~~the errors in the height of the measurements (z_1 and z_2) were negligible and that the error in $f(z, \Psi)$ solely depend on the errors in the stability corrections. Following Wolff et al. , we assumed that the stability corrections have a relative error of 10%.~~

~~The random error of the half-hourly uncorrected EC NH_3 fluxes is estimated in EddyPro following Finkelstein and Sims . To determine the random error of the WPL corrected NH_3 fluxes, is rewritten as a sum of four terms F_1, F_2, F_3 and F_4:~~

$$F_{EC} = A\overline{w'\rho_A'} + AB\mu\frac{\overline{\rho_A}}{\overline{\rho_d}}\overline{w'\rho_v'} + AC\frac{\overline{\rho_A}}{\overline{T_a}}\overline{w'T_a'} + AC\mu\frac{\overline{\rho_v}}{\overline{\rho_d}}\frac{\overline{\rho_A}}{\overline{T_a}}\overline{w'T_a'} = F_1 + F_2 + F_3 + F_4 \quad \text{Eq. 4}$$

~~The random error of the WPL method corrected NH_3 fluxes ($\sigma_{F_{NH_3,HT}}$) is computed as follows:~~

$$\sigma_{F_{EC}} = \sqrt{\sigma_{F_1}^2 + \sigma_{F_2}^2 + \sigma_{F_3}^2 + \sigma_{F_4}^2} \quad \text{Eq. 5}$$

~~Here, the term F_1 represents the NH_3 flux term in the WPL correction, whose random error (σ_{F_1}) largely follows the random error of the HT NH_3 fluxes ($\overline{w'\rho_A'}$) from EddyPro. The term F_2 represents the water vapour term, and F_3 and F_4 together are the heat terms in the WPL correction, respectively. To determine the random error of each term, the relative errors of the included variables are propagated. The relative error of the NH_3 density (ρ_A) from the HT reported by the manufacturer is 15% (Wang et al., 2021). The relative errors of the dry air density $\overline{\rho_d}$, water vapor density $\overline{\rho_v}$ and air temperature $\overline{T_a}$ from sonic#1 are estimated to be 5%, 5% and 1%, respectively . Finally, the relative random errors of the water vapour flux ($\overline{w'\rho_v'}$) and the sensible heat flux ($\overline{w'T_a'}$) were taken from EddyPro~~1.2 of the supporting materials.

3.5 Footprint analysis

The footprint of the EC fluxes showing the contributing area of measured fluxes was analysed following the method from Kljun et al. (2015). Inputs for this method include the EC measurement height ($z = 2.80$ m), roughness length (assumed to be 0.15 times canopy height), friction velocity (u_*), the Obukhov length, the standard deviation of the lateral wind (v) component, wind direction, mean wind speed, and the boundary layer height. Apart from the boundary layer height, other parameters were measured by the EC system. The hourly boundary layer height data was obtained from Climate Data Store (CDS) source (ERA5 hourly data: https://cds.climate.copernicus.eu/cdsapp#!/dataset/reanalysis-era5-single-levels, last access date: 1 Feb 2022) and the hourly values were linearly interpolated to half-hourly values for the footprint calculation. The flux footprint prediction (FFP) method (http://footprint.kljun.net, last access date: 1 Feb 2022) was used for coding and plotting. Here, footprints were only determined for EC NH_3 flux after quality filtering (see Sect. 3.3). No separate footprint analysis was done for the AGM fluxes.

4 Campaign results

4.1 NH_3 concentrations

4.1.1 MiniDOAS intercalibration

The lab calibration procedure of both individual miniDOAS instruments is described in the instrument section (Sect. 3.1.2~~), with a validated accuracy of better than 3%.~~). Here, ~~only~~ the ~~results~~result of the intercalibration ~~of the two instruments~~ in the field ~~are~~is shown, which aims to increase the precision of the concentration difference measurement further.

~~With the instruments placed in cross-position, intercalibrations~~ Intercalibration measurements were taken in three periods: at the beginning and end of the campaign and once during the campaign. In total, 35% of the 7-week uptime was spent ~~for the intercalibration during the campaign.~~

~~For intercalibration purposes, a concentration gradient is acceptable in these measurements, but this gradient needs to be the same over the full length of the paths. Therefore,~~on intercalibrations. The data was filtered for well-mixed situations ($u_* > 0.1$ ms^{-1}) and obstacle-free wind directions (green and light green~~).~~) in order to obtain homogenous concentration gradients along the path. Figure 5 shows a ~~scatterplot~~scatter plot of the obtained concentration measurements by both instruments matching these requirements.

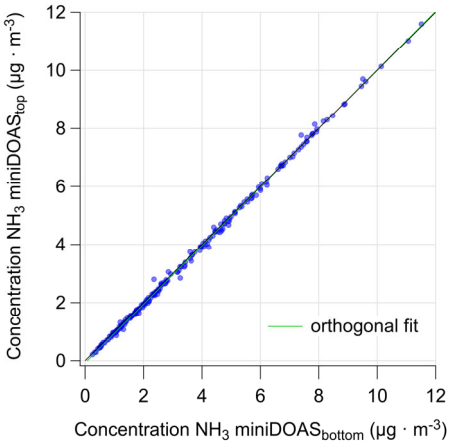

Figure 4.~~ Scatterplot~~. Scatter plot of data obtained by the two miniDOAS instruments during all three cross-periods. Data was filtered to include only obstacle-free wind directions and turbulent conditions ($u_* > 0.1\ m\ s^{-1}$). Using an orthogonal fit, an offset of 0.07 ± 0.01 µg m^{-3} and a slope of 1.009 ± 0.002 (the green line) was found.

~~With the obtained offset and slope between the systems, the concentrations of miniDOAS$_{top}$ were corrected, in order to get a scatterplot with offset 0 and slope 1 after correction. Next, the same minor correction factors~~The offset and slope correction were applied to the concentrations of miniDOAS$_{top}$ over the full campaign. The standard deviation of the residuals was used as an estimate of the remaining random uncertainty in the concentration difference $c_{NH_3}(z_2) - c_{NH_3}(z_1)$ after correction. ~~The~~This random error ~~of the miniDOAS NH$_3$ concentration differences $\sigma_{c_{NH_3}(z_2) - c_{NH_3}(z_1)}$ in~~ was determined to be 0.088 µg m^{-3}.

~~The concentration differences between the miniDOAS paths during the three cross periods are shown in . The blue elements of the time series meet the selection criteria mentioned above. For these blue data points, statistics are given separately for the three periods.~~

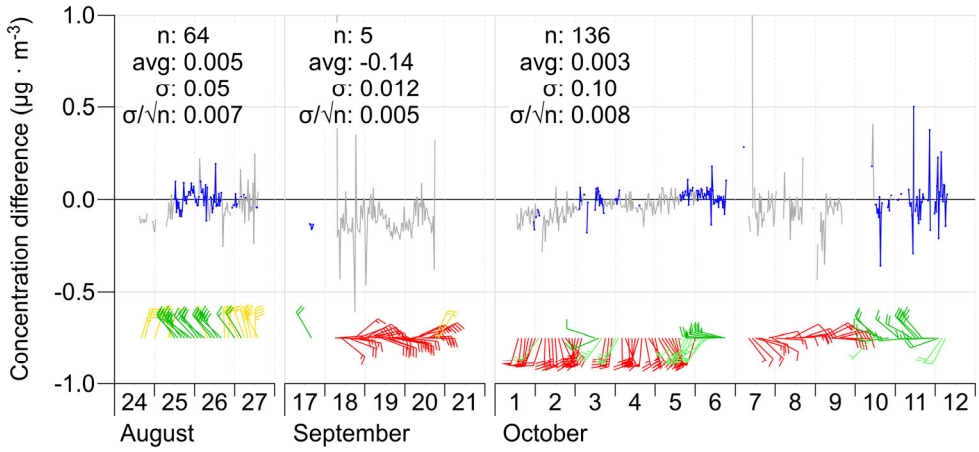

~~**Figure . Top trace: Time series of de observed NH_3 concentration difference between the two miniDOAS instruments during the three cross periods, after correction of the top miniDOAS values based on the intercalibration as described in the text. Only data during well-mixed conditions ($u_z > 0.1\ ms^{-1}$) are shown. Measurements from obstacle-free wind directions are blue, other directions are grey. The sets of statistics given in the plots apply to the blue measurements only. Bottom trace: 30-minute wind vectors colour-coded with the wind sectors described earlier. Wind speed is indicated as barbs, as used on meteorological maps. To reduce clutter, only 1 in 4 wind vectors are shown.**~~

~~In the first cross-period, the average half-hourly difference was 0.005 ± 0.007 µg m^{-3} and the standard deviation was 0.05 µg m^{-3} ($n = 64$). For the last cross-period, these values were 0.003 ± 0.008 µg m^{-3} and 0.10 µg m^{-3} ($n = 136$), respectively. The average only shifted by 0.002 µg m^{-3} between cross-periods 1 and 3. This is well within the combined uncertainty range. The spread of the half-hourly values has increased from 0.05 in cross-period 1 to 0.10 µg m^{-3} in cross-period 3. This increase was likely at least partially caused by the gradual decay of the lamp intensity, causing a larger measurement error. The 'ageing' of the field reference spectrum may also have played a role here, but this was not studied further.~~The results of the intercalibration periods are discussed in section S1.3 of the supporting materials. The conclusion is that, over the full campaign period, the zero-level of the difference measurement has been stable, and the individual difference measurements showed a typical spread of 0.1 µg m^{-3} or less.

~~The second cross-period contained almost no valid data points, as the wind during this cross-period was coming from the direction of the largest obstacle of all: the 213-meter mast. Its impact on the analysis above was therefore almost zero. The data during this cross-period show how large the magnitude of the effect of upwind obstacles can be. The grey points taken during this cross-period differed systematically from zero by about 0.2 µg m^{-3}, reflecting that the gradients were different at different locations along the paths.~~

4.1.2 HT concentration corrections

The HT NH_3 concentration measurement contained a considerable amount of gaps in the data (21% during the 5-week uptime). These gaps largely occurred during rain and mirror cleaning afterwards. At the start of the campaign, the HT instrument had an offset of about -7 µg m^{-3} (data not shown). After the campaign, the analyser was recalibrated in the lab and the 'zero' was found to be -6.3±0.3 µg m^{-3} when flushing pure nitrogen gas for 6 hours through the calibration cell while the temperature was kept constant at 17 °C. Before temperature correction, raw HT and miniDOAS$_{top}$'s average difference was -5.3 µg m^{-3} (range -15 to 6 µg m^{-3}, $n = 1180$) during the overlapping period of the campaign. The raw half-hourly HT NH_3 concentrations showed inconsistent differences compared to the miniDOAS concentration levels, which varied with air temperature. After applying a third-order polynomial fit of the HT-miniDOAS concentration difference versus temperature, the corrected concentrations for

HT were finally obtained (Figure ~~S4~~S7). Tempature mainly impacted on the offset of its concentration and it seemed to have a negligible influence on the span of the HT's concentration (slope ≈ 0.97, Figure 7).

4.1.3 Comparison miniDOAS and HT concentrations

After application of the temperature correction on the NH_3 concentrations of the HT, the concentration of the two instruments were very similar ($R^2 = 0.97$, Figure 7). Furthermore, the time series of the corrected NH_3 concentrations from both instruments captured the same temporal pattern and peak events. The highest concentrations ~~were~~are observed ~~by both systems at noon~~during night-time when ~~air temperature reached~~ the ~~highest level~~boundary layer height is small and vertical mixing is limited. During daytime the concentrations decrease due to the rise of the ~~day~~boundary layer and the increased vertical turbulent transport (Figure 8).

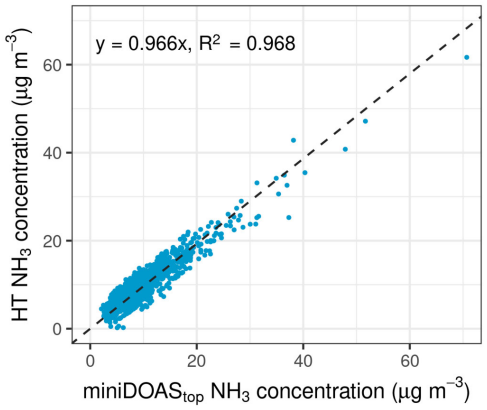

Figure 5 ~~Scatterplot~~ Scatter plot of the NH_3 concentrations from the $miniDOAS_{top}$ and the temperature corrected HT instrument during parallel measurements (correlation line was forced through the origin).

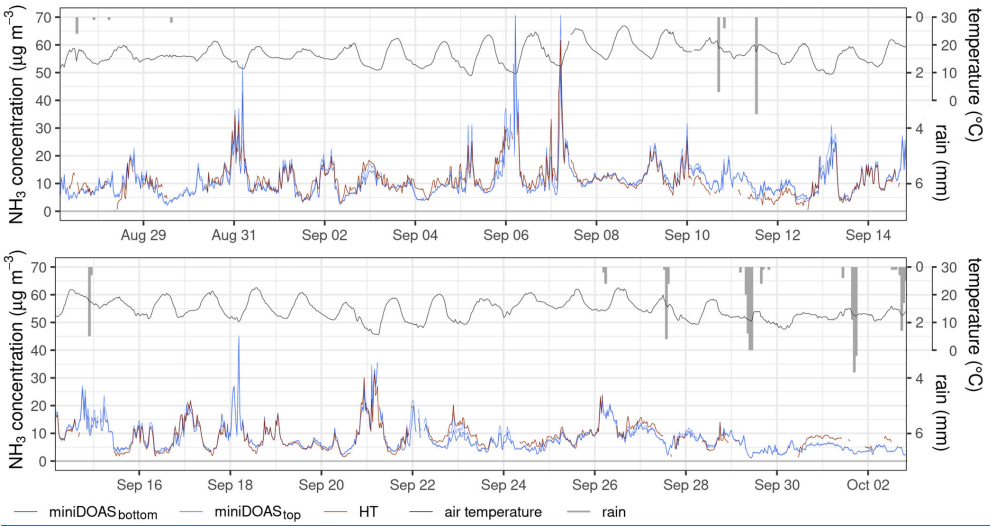

Figure 6. Time series of the measured, unfiltered NH_3 concentrations after temperature correction from the HT (red) and the

miniDOAS instruments (dark blue for the bottom one; light blue for the top one) in µg m^{-3}, the hourly ambient temperature (black) in °C and the amount of rainfall (grey bars) in mm.

4.2 Uptime, filtering and quality control

For the AGM method, the vertical NH_3 concentration gradient measured by the miniDOAS instruments and the transfer velocity from the sonic #1 anemometer were used to determine the NH_3 flux. Figure ~~S5a~~S8a in the supplementary materials shows the full time series of the NH_3 flux derived using the miniDOAS setup. The miniDOAS setup had an uptime of nearly 100% over the full campaign (1142 hours). Except for the 35% intercalibration period, 80% of the remaining parallel measurements (597 hours) were left after filtering out low turbulent mixing conditions ($u_* < 0.1$ m s^{-1}) and outliers. For the EC NH_3 flux measurements, Figure ~~S5b~~S8b shows the full time series. The uptime of the HT instrument was 79% during the 5-week field operational period (685 hours). After filtering for fluxes with poor quality flags, $u_* < 0.1$ m s^{-1} and outliers, 59% of the valid observations remain (516 hours). ~~At last, after filtering all measurements on September 11th (discussed in Sect), 424 overlapping hours were left for flux comparison between two instruments.~~

~~**4.3 Comparison of the AGM and EC fluxes**~~

~~The NH_3 fluxes from the two methods are shown in . Here, the EC fluxes corrected for flux damping in EddyPro are shown, which is considered as a reference method.~~ Observations on the 11th of September were excluded due to ~~remarkable~~ large differences between the measured fluxes on that day, although they originated from green wind directions. We assume this was related to manuring at the adjacent field that might have disturbed the footprint homogeneity of the flux but we have no evidence to support that. After filtering, 848 overlapping half-hours were left for flux comparison between two instruments.

4.3 Comparison of the AGM and EC fluxes

Both NH_3 fluxes are shown in Figure 9. Here, the EC fluxes corrected for flux damping in EddyPro are shown, which is considered as a reference method. After quality control filtering, the EC and AGM fluxes have a similar range and pattern. Within the green and light green sectors, the highest NH_3 emission measured with the AGM setup was 0.18 µg m^{-2} s^{-1} and deposition was 0.15 µg m^{-2} s^{-1}. The highest observed NH_3 emissions with the EC setup was 0.16 µg m^{-2} s^{-1} and deposition was 0.10 µg m^{-2} s^{-1}.

At the start of the measurement period, the AGM and EC fluxes were quite different. During the first days, the miniDOAS system presented NH_3 deposition, while the HT showed NH_3 emissions. In this period, the prevailing winds were from the north/northeast, categorised as yellow (see Figure 1), where sheep were occasionally located upwind of the instruments. This may have caused inhomogeneity of the source/sink pattern within the footprint area (see below), which would have violated the AGM/EC calculation assumptions. Furthermore, the NH_3 concentrations during this episode were relatively high as manuring activities were still allowed until 15 September on the grasslands surrounding the measurement site. ~~The~~ In the green and light-green wind directions, the NH_3 fluxes from the two methods compared well ~~during the second half of the measurement campaign during times~~after September 20th when ~~the airflow was unobstructed (green and light green wind categories).~~little or no effect of manure application should be present.

~~Figure S6 in the supplementary materials shows cumulative fluxes using only data after September 15, when manure spreading was not allowed anymore.~~ Considering only high-quality measured fluxes during this period, the cumulative daily fluxes of the AGM and EC were ~~likely within~~in general similar, with typical differences in the order of ~10~~%. The daily~~% (Figure S9). When looking at the cumulative ~~NH_3 fluxes illustrated that~~flux over the ~~differences between the two methods can largely be traced back to~~ full period however, a larger difference is observed. This difference appears stepwise on a single day, September 24th. On this day, and only during a few hours around noon, we see a much larger flux observed by EC compared to AGM.

Most likely, the discrepancy is caused by footprint issues in combination with very local emissions. Unfortunately, we lack the ~~daily cumulative AGM fluxes may have been substantially larger than the cumulative EC flux~~means to validate this assumption.

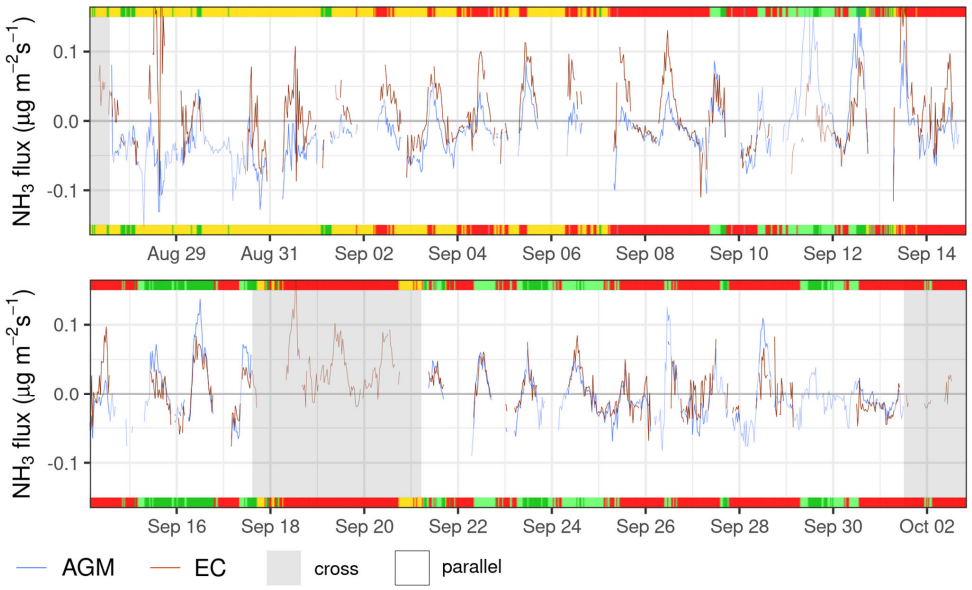

Figure 7. Timeseries of the NH_3 fluxes of AGM with miniDOAS instruments (blue) and the EC method from the HT (red). Positive fluxes indicate emissions, negative fluxes deposition. The colours in the upper and lower borders indicate the prevailing wind directions from Figure 1. The intercalibration periods for the miniDOAS instruments are shown against a grey background. The thick lines indicate the NH_3 fluxes that were left for intercomparison after all filters were applied.

Figure 10 shows the comparison of the EC (EddyPro calculated) and AGM NH_3 fluxes per categorized wind direction. There is a strong correlation ($r = 0.87$) between the EC and AGM NH_3 fluxes at times where the airflow was unobstructed, i.e., when the wind came from the directions categorized as green. In this category, the differences between the EC and AGM NH_3 fluxes were relatively small (RMSE = 0.027, bias = 0.012), too. There is a moderate correlation between the EC and AGM NH_3 fluxes in the light green ($r = 0.71$) and the red categories ($r = 0.69$). In both the green and light-green categories, the AGM based fluxes were approximately 30% above the EC based levels (slope = 1.3 (green) and slope = 1.35 (light green)). In the red category, the airflow was partially obstructed by large objects ~~(e.g., the 213 m mast, trailers and containers with measurement devices).~~ In this category, the EC fluxes were generally larger than the AGM fluxes (slope = 0.64), but relatively small differences (RMSE = 0.034, bias = -0.016) between the EC and AGM NH_3 fluxes were found still. The poorest agreement ($r = 0.33$, RMSE = 0.072, bias = -0.045) between the two methods is found for the yellow wind direction category. In this category, the HT often observed NH_3 emissions while the miniDOAS setup observed deposition of NH_3.

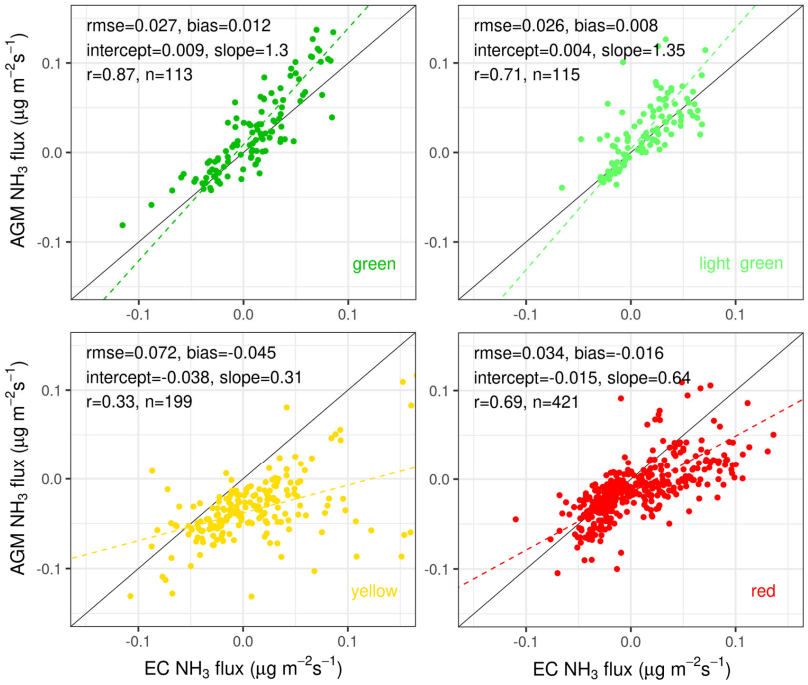

Figure 8 Comparison of the AGM NH3 fluxes from the miniDOAS instruments and the EC NH3 fluxes from the HT per categorized wind direction (see Figure 1).

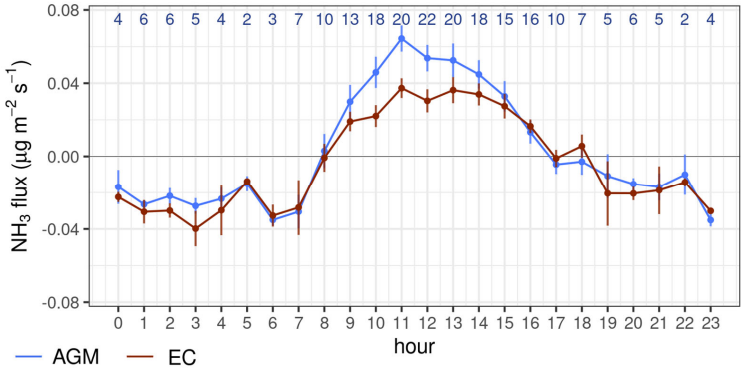

Figure 9. Mean diurnal cycle of the EC and AGM NH_3 fluxes. Positive flux is emission, negative flux is deposition. The error bars indicate the standard error of the hourly means $(\sigma/\sqrt{n})$. The number of hours averaged are listed in blue text at the top. Here, filtered NH_3 fluxes from only the green and light green wind directions where both systems have a valid flux observation were used. Data from the 11th of September is excluded, too, due to a potential emission event causing footprint heterogeneity.

The two methods showed a similar diurnal pattern using ~~filtered~~ NH_3 fluxes ~~only~~ from the green and light green wind directions (Figure 11). NH_3 was generally emitted during the day and deposited during the night. Between 10 ~~am~~:00 and ~~2 pm~~14:00, the AGM fluxes were a factor ~1.7 higher than the EC fluxes. Figure ~~S7~~S10 in the supplementary materials shows the diurnal

pattern using only data after September 15. The mid-day differences between the two are smaller, but still exist, even though manure spreading was not allowed anymore.

4.4 Uncertainty analysis

Figure 12 shows the random errors of the AGM and EC NH_3 fluxes and the contribution of different components to the error. The random errors of the two showed a similar range of values. On average, EC NH_3 fluxes had a slightly lower ~~estimated~~ error. The mean random error (1σ) of the AGM NH_3 flux was ~~9.8~~15.0 ng m^{-2} s^{-1} (median 7.6~~4~~ ng m^{-2} s^{-1}), while the mean random error of the EC NH_3 fluxes amounted to 5.5 ng m^{-2} s^{-1} (median 4.1 ng m^{-2} s^{-1}). The mean and median relative random errors were ~~87~~89% and ~~23~~24% for the AGM flux ~~(excluding cross-periods)~~ versus 61% and 15% for the EC flux.

The random errors of the AGM fluxes showed a clear diurnal pattern. During the daytime, the random errors were relatively large and peaked around noon, because the observed gradient was the smallest at this time. As a result, the measurement error in the NH_3 concentration differences ~~from the miniDOAS instruments~~ dominated. During the night, the random errors were relatively small~~.~~; here, the errors in the ~~measured~~ u_* values ~~from the sonic anemometer~~ had a relatively large contribution ~~to the total random error. The contribution of u_* was relatively large when NH_3 was deposited at this site, i.e. the measured NH_3~~ . As a consequence, especially deposition estimates were ~~especially~~ sensitive to the random error in u_*. The largest random errors in the NH_3 fluxes largely ~~coincided with moments where~~took place when the error in the stability correction takes over, i.e. when a substantial stability correction was applied to the measurement heights of the miniDOAS instruments. This occurred occasionally during night-time, usually around midnight. Compared to the random error of the AGM NH_3 fluxes ~~of the miniDOAS instruments~~, the diurnal cycle of the random error in the EC NH_3 fluxes ~~of the HT~~ was less apparent. The contributions of the heat terms in the WPL correction to the total random error were negligible. The contribution of the error in the WPL water vapour term can be quite substantial (max. ~75%) in incidental cases but is generally between zero and ~20% during daytime.

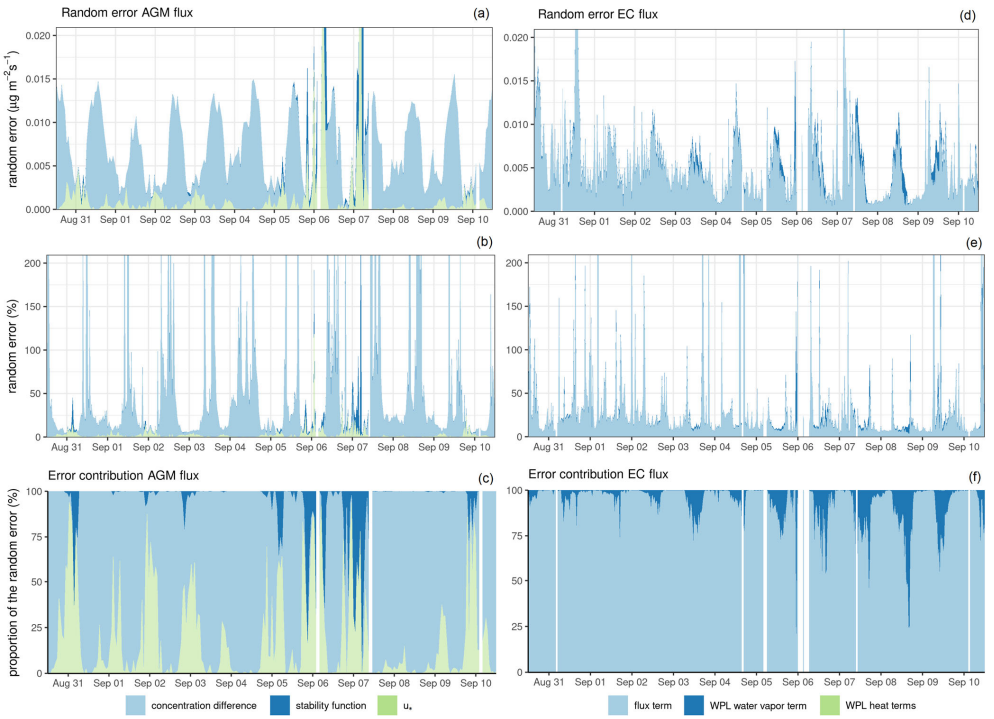
Random error AGM flux
(a)
Random error EC flux
(d)
random error (μg m⁻²s⁻¹)
(b)
(e)
random error (%)
Error contribution AGM flux
(c)
Error contribution EC flux
(f)
proportion of the random error (%)
Aug 31 Sep 01 Sep 02 Sep 03 Sep 04 Sep 05 Sep 06 Sep 07 Sep 08 Sep 09 Sep 10
concentration difference
stability function
u*
flux term
WPL water vapor term
WPL heat terms

620

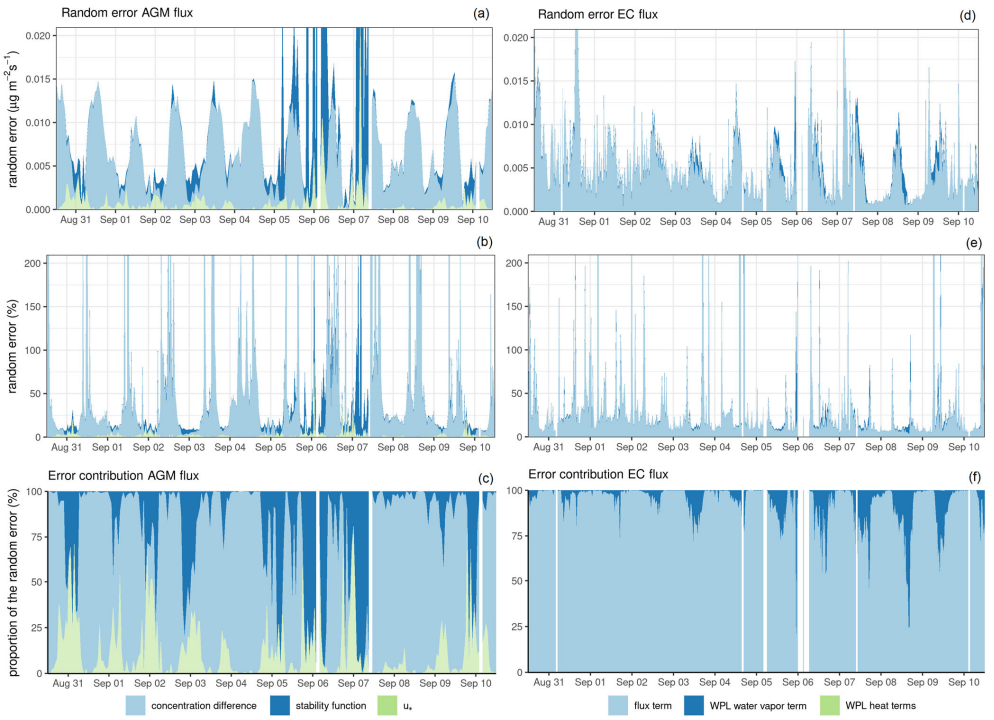
Random error AGM flux
(a)
Random error EC flux
(d)
random error (μg m⁻²s⁻¹)
(b)
(e)
random error (%)
Error contribution AGM flux
(c)
Error contribution EC flux
(f)
proportion of the random error (%)
Aug 31 Sep 01 Sep 02 Sep 03 Sep 04 Sep 05 Sep 06 Sep 07 Sep 08 Sep 09 Sep 10
concentration difference
stability function
u*
flux term
WPL water vapor term
WPL heat terms

Figure 10. The absolute and relative random errors and the corresponding error contributions (in % of the random error) of the AGM (a, b, c) and EC (d, e, f) NH_3 fluxes from August 31st to September 10th. For the EC fluxes, the light blue component (flux term) refers to F1 in Eq. 4, based on fluxes determined using EddyPro, taking into account the damping correction and term A from Eq. 4.

4.5 Footprint analysis

The footprint of the EC NH_3 fluxes was computed at sonic #1's height using the method from Kljun et al., (2015) and shown in Figure 13a for all wind directions and in Figure 13b for only the green and light-green sectors. Overall, 80% of the flux originated from an area within approximately 100 meters distance from the measurement devices. Furthermore, the influence of the 213 m mast seems visible and reduces the footprint to the southeast. Because the highest measurement point has the largest footprint, the footprint of the miniDOAS instruments, especially $miniDOAS_{bottom}$, will be substantially smaller. The measured fluxes are assumed to be representative of the footprint area. The largest footprint area determines the outside perimeter of the area within which the landscape should be homogenous. If that is not the case it can be expected that the AGM and EC methods will end up with different results.

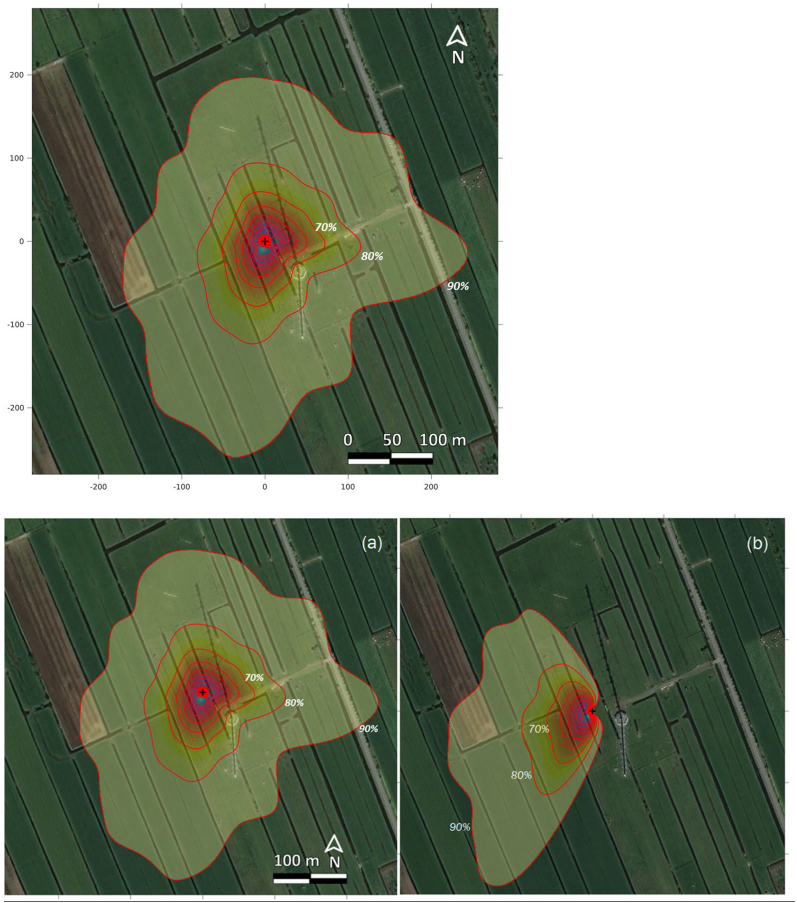

Figure 11. EC footprint for (a) all wind sectors and (b) the green and light-green wind sectors Footprint climatology estimate of the EC measurements ($z = 2.80$ m).The red curves are at 10% footprint contour lines. Background map data: Microsoft, CNES Distribution Airbus DS

4.6 Damping correction methods: TEO versus ICO for EC flux

To evaluate the effect of damping on the EC flux, both the theoretical method from EddyPro (TEO) and the empirical method (ICO) were used. In the results above we use the EddyPro theorical approach (Table S1) since we consider that is the 'standard' evaluation method. The comparison showed that theoretical flux correction factors in EddyProTEO corrections are larger than the levels obtained for the empirical (ICO) factors for CO_2, H_2O, and NH_3 (Figure S8). The first cause for that is thatS11). The sensible heat flux cospectrum indicates that the theoretical Kaimal cospectrum in TEO does not represent the turbulent characteristics of the sitessite well enough (Figure S9). If applyingS12). Application of the ICO method on the HT data, the correlation however decreased correlations with the AGM results gets worse in both the light green and green wind sectors (Figure S10S13). The ICO method seems to be conceptually better. However, ~50% of the dataset had to be corrected using daily median values, because the measurement-based ogives were noisy (caused by low flux conditions). We therefore decided for this relatively short campaign to still use the TEO method for the flux comparison with AGM method.

The effect ofdamping is affected by both the sensor separation on the damping was evaluated. We tried to split the effect of the and the sensing volume size. The HT and the effectcombination of thesonic #1 and LI-7500DS were 1.5 m sensor separation between the HT and the sonic#1 on the total flux dampingapart during the entire campaign period. This was done with the ICO method by comparing the damping factors when two sonics were both installed shortly at the site 2 days before the end of campaign. For sonicUsing sonic #1 data at 1.5 m from, the HT instrument median flux damping of NH_3, CO_2, and H_2O were 37%, 1%%, and 1%, respectively. according to ICO method. For the second sonic anemometer, sonic#2 #2 which was installed at the end of the campaign for 2 days at 0.40 m ofdistance to the HT instrument and 1.35 m to the LI-7500DS the empirical methodICO gave 16%, 32%, and 31% for NH_3, CO_2, H_2O damping. The effect of So the separation between the HT and the sonic #1 caused ca. 20% extra damping for NH_3 flux, while. Separating the LI-7500DS and sonic #2 by the same distance caused 30% extra flux lossesdamping for both the water vaporH_2O and CO_2 flux. That could be explained because the HT has a 4 times longer vertical path length than the LI-7500DS sensor (0.50 m *vs.* 0.125 m) in which higher frequencies will be damped anyway.

To further check whether the TEO method can properly correct the sensors separation impact during the entire campaign period, especially between HT and sonic#1, this method was applied to compare the damping effect on both sonics in the short period as well. With the TEO method,

The TEO method, applied for the two days with both sonics available, gave median damping factors of 41%, 14% and 14% for NH_3, CO_2, and H_2O were 41%, 14% and 14% using sonic #1 as reference and 20%, 38%, and 37% using sonic #2. TheBoth TEO methodand ICO methods produced the same damping difference between sonic#1 and sonic#2the two sonics for NH_3 flux as the ICO method (*ca.* 20%). After implementation of the damping correction, the As a consequence, the corrected NH_3 fluxes obtained simultaneously with the HT and sonic #1 or sonic #2 were the same (see Figure S11). However, byS14) suggesting the damping correction provides reasonable flux estimates. When comparing the fluxes generated throughwith sonic #1 during the entire campaign period, the averaged theoretical dampingTEO corrections for all gases were relatively larger than the experimentalICO ones (see Figure S8), such asS11). For NH_3 flux losses were 39% versus 28%, respectively. Surprisingly, even without extra distance separation between LI-7500DS and sonic #1, the TEO method still generatedsuggests 12% correction for the H_2O and CO_2 flux and water vapor flux, while ICO method results suggested the neededonly suggests 2-3% damping correction was much smaller, only 2-3% onas average for the entire period.

5 Discussion

In this experiment, we had the unique opportunity to use two newly developed instruments that share one essential feature needed to improve NH_3 flux measurements: ~~neither of the instruments has an inlet line.~~both are open path. These two instruments provided independent data for the flux estimate.

5.1 Field performance

~~The field performance of the miniDOAS and HT setup was assessed during this campaign.~~ The miniDOAS system was steadily housed in an air-conditioned container, and was operational and measuring close to 100% of the campaign period. In the campaign, 35% of this time was spent on intercalibration of the two miniDOAS instruments, and the rest on flux measurements. Towards the end of the campaign, after the HT had been removed from the field, the miniDOAS instruments were intentionally kept in cross-setting ~~to confirm stability of the baseline of the concentration difference~~ for two extra weeks. These intercalibration measurements confirmed the baseline stability of the NH_3-difference measurements was better than 0.002 µg m^{-3} drift over a seven-week period. In future applications, the frequency and duration of the inter-instrumental calibration ~~of the two miniDOAS instruments~~ can be further optimized, increasing the percentage of operational flux measurements to well above 65%. The miniDOAS optical system was almost insensitive to degradation, although the parabola mirror and the lamp may need replacement after about a year. Hence, we conclude that the miniDOAS gradient setup is field ready in its current configuration, also for longer-term measurements.

For the HT, ~ 21% missing data were caused by ~~raindrop~~raindrops or dew on the optical mirrors, and the coating material of the mirror gradually deteriorated along time over the five-week period presumably due to rain as well. In addition, the HT instrument needed regular operator intervention (e.g. mirror cleaning). To make the instrument suitable for longer-term monitoring, in particular in areas with frequent rainfall, this needs to be addressed in future versions.

5.2 Flexibility in application

For operation in the field, the miniDOAS system requires at least about 10 meter, preferably 20 meter, of ~~steady~~relatively flat and horizontal surface between container and retroreflectors. It also requires structural stability to maintain the alignment between the miniDOAS instruments and their retroreflectors. That is feasible for ground-level operation but more difficult for a site with tall vegetation, for example when evaluating deposition above forest canopies from a tower. Besides, the miniDOAS instruments also need ~ 200 W at 230 V each, and are operated from a container ($2 \times 2 \times 2$ m) with air conditioning. Hence, its operation depends on a substantial mains power supply. The light-weight and portable HT instrument, on the other hand, currently only needs a 12 V, 50 W power supply permitting use at remote sites without access to mains power. It can be supported by a solar panel and a battery.

5.3 Concentration comparison

A substantial and varying discrepancy in NH_3 concentrations was found between the HT and the miniDOAS at similar measurement heights (average discrepancy -5.3, range -15 to + 6 µg m^{-3}). The miniDOAS instrument was initially designed for measurement of the absolute concentration level. It is currently used for concentration monitoring in the Netherlands and has a validated accuracy of better than 3%. Therefore, we concluded that the observed discrepancy was caused by a substantial and varying offset in the concentrations recorded by the HT, which correlated with the changing ambient air temperature (Figure ~~S4~~S7, $R^2 = 0.68$). In an earlier study testing the performance of the HT, Wang et al. (2021) compared measured NH_3 concentrations of the HT to those of a Picarro closed-path laser-based NH_3 analyser under steady lab conditions. The difference was within 10% during a 14-h experimental period. However, the indoor air temperature during that relatively short experiment would likely have been fairly stable, so any potential impact of temperature variation on concentration measurements by the

HT could not easily be detected. In our field experiment, after applying the correction function to the HT concentrations using the air temperature data, the agreement of concentration between the miniDOAS and HT was substantially improved. It remains to be seen if the parameters for this temperature correction function change over time and under different temperature ranges. Having the absolute concentration level right is especially important when using it to interpret the flux data beyond the net flux, and also when calculating deposition velocities. Since not all users have a separate, reliable concentration measurement alongside the HT in the variable field conditions, it is important to improve the accuracy of measured concentrations of the HT itself. The effect may be caused by the external heat-exchange unit of the HT, which does not provide a temperature lock. To reduce the influence of variable temperatures on the absolute concentrations, a Peltier stabilised external cooler could be tested along with the HT.

5.4 Flux comparison

We evaluated the AGM and EC fluxes using standard, established analysis techniques for both. When the wind came from the "green" sectors – where upwind terrain was relatively homogenous and obstacle-free~~,~~ – the overall pattern of the fluxes and the diurnal pattern agreed remarkably well between the DOAS-AGM and the HT-EC setups. Moreover, the fluxes showed a clear bidirectional behaviour switching between emission and deposition and also between day and night. Larger differences between the AGM and EC fluxes were observed for the other wind directions (Figure 10). The discrepancies between the AGM and EC fluxes can have several causes.

When measuring fluxes, the terrain upwind of the instruments ideally needs to be obstacle-free. Obstacles interfere with both measurement techniques, as they affect atmospheric turbulence pattern and disturb the NH_3 gradient. This condition was not met for all wind directions. In our case, all instruments were ~ 60 m away from the 213 m high tower especially when the wind came from the southeast (the red wind sector). The fluxes were less comparable between AGM and EC than when fluxes originated from an obstacle-free area (the green wind sector), but the correlation was still modest ($r = 0.69$) as both measurement sets were under the similar influence from such a big obstacle. When the wind blew from the north, obstacles in that direction were smaller, but still agreement between fluxes from AGM and EC was poorest ($r = 0.33$) and even occasionally showed fluxes in oppositive directions. This may have indicated that under such conditions, the heterogeneity of footprint area, for example caused by sheep grazing the research site, could have played a bigger role on the fluxes measured ~~fluxes~~ by the two systems.

Both the EC and AGM techniques assume spatial homogeneity of the surface-atmosphere fluxes and terrain within the footprint. Due to the differences in measurement height and path- versus point-sampling, the AGM and EC setups 'see' different areas (Loubet et al., 2013). The footprint analysis for the EC method showed that measurements were representative of the terrain up to approximately 100 m upwind (Figure 13). Because of the lower measurement heights, the footprint of the AGM setup is expected to be smaller. In addition, the footprint of the upper and lower miniDOAS instruments was different. Thus, if either the terrain or fluxes were inhomogeneous, the AGM and EC setups may have captured different NH_3 fluxes. At this measurement site, spatial homogeneity may partly be violated by the ditches in the terrain. Direct emissions may be spatially inhomogeneous due to manure or fertiliser application or excreta from grazing animals. Fertilization and grazing also impact the nitrogen status of the vegetation. This leads to an enhancement of the nitrogen content of the vegetation, which could lead to stomatal emissions of NH_3 in daytime. To confirm the occurrence of potential stomatal emissions of NH_3, however, further interpretation of the measured NH_3 fluxes is needed. This is considered beyond the scope of this study but will be addressed in an upcoming paper.

We found that HT concentrations can differ substantially from miniDOAS concentrations. The differences were strongly linked to ambient temperature. In our current analysis, we treated these differences as a temperature-dependent offset. As ambient temperatures only changed gradually in time, so did the applied offset in the correction. As a consequence, this correction has

virtually no impact on the HT flux measurement, as the flux measurement is based on observed concentration variations on a short timescale.

It is however not clear if the effect of temperature is limited to inducing just an offset in concentration. There could also be an influence on the span: at higher temperatures the HT might be more, or less, sensitive to NH_3. This would affect the flux measurement by the same factor and could be an explanation for the discrepancy in flux between miniDOAS and HT during daytime (Figure 11).

To eliminate this possible source of discrepancy, further studies to the cause and the exact effect of the temperature on the offset and slope of the HT calibration are necessary. The cause of the sensitivity to ambient temperature may be instrumental, or spectral broadening.

In this paper, commonly-used flux calculations were used for both techniques. For the AGM method, standard calculations were used that are well established and ~~has~~have been used for over ~~two~~three decades now (e.g. Businger, 1986). For EC flux, the standard analysis method in EddyPro was used, including the theoretical correction for high-frequency losses (TEO). Current instrument setups, however, are different from regular AGM and EC instruments (path versus point for miniDOAS, larger measurement volume for HT) and are applied to a new gas. These analysis techniques may therefore need adaptations. For example, we also tested an alternative experimental analysis method (ICO) to correct high-frequency losses for the EC and found different flux results.

The effect of the theoretical damping correction in EddyPro adds about 40% to the raw flux data. The estimate of Moncrieff et al. (1997) relies on the comparison of the theoretical frequency distribution of the NH_3 flux considering the damping through spectral transfer functions with a theoretical turbulence contribution per frequency. When using the empirical (ICO) method as described by Wintjen et al. (2020), using the cospectra for both the temperature and NH_3 turbulent data and matching these two the damping effect would only be 30% (about half of that due to sensor separation and half due to the sensor size). In that case, the mismatch between the AGM and EC fluxes would increase to 50% instead of 30% (slope of the x-y fit in the green sectors in Figure 10 and Figure ~~S10~~S13). Since we do not have a very large dataset and because the empirical method can only properly run on the subset of the data that has fluxes large enough to make a reasonable spectral distribution, the fit of miniDOAS vs. HT shows more scatter (Figure ~~S10~~S13). The benefit of the theoretical approach in EddyPro is that the theory is always available since it relies only on the arrangement and dimensions of the instrument. Therefore, we choose to present the comparison based on the EddyPro calculation but strongly advise further evaluation of the damping calculation method. Similar advice is given for the AGM method, where almost everyone uses the standard stability correction functions and these bring a generalisation that might be not fully representative at a given measurement site. Hence, it is not surprising to find that when comparing the ICO method NH_3 flux to the theoretical AGM method, the correlation is worse.

Part of that damping was related to the sensor separation, which was outlined above. Reducing the distance between the sonic anemometer and gas analyser to closer than the 40 cm heart-to heart distance we used is not recommended, because then the instruments can be too close to touching each other. The damping correction might get smaller but the HT instrument is likely to distort the airflow due to shadowing effects of the sonic transducers (Horst et al., 2016).

5.5 Outlook

For the Netherlands, the main goal for these measurement sets is to evaluate the deposition levels of NH_3 in Natura 2000 areas (European Union, 1992). The flux levels in these areas are generally low and less complex in temporal structure. Little or no (re-)emission is to be expected. To further test the performance of the flux instruments for these conditions, the comparison of the miniDOAS and the HT instrument should be continued at more homogeneous sites. Attention should be given to avoid nearby obstacles and nearby animal emission sources within the footprints. These intercomparisons could also include further studies into the temperature sensitivity of the HT, and tests for remedies thereof in future versions.

The stability of the miniDOAS instruments need to be confirmed for longer-term monitoring applications. In particular, the duration and frequency of the intercalibration periods needs to be optimized to allow a larger fraction of the measurement time in flux-mode.

In a follow-up study, the effect of different flux data processing algorithms can be further quantified. These studies need to address the different processing options for both techniques and their effect on the calculated fluxes. For consistency, we suggest processing different techniques on a similar level of complexity, i.e., representing the local atmosphere on the same level of detail and using either theoretical or site-specific corrections. For example, if actual, measured turbulence spectra are used in the EC-analysis, locally-derived flux-profile relationships should be used in the AGM-analysis.

6 Conclusions

We compared two novel open-path optical instruments to measure NH_3 concentration and flux during a 5-week comparison period at Cabauw, the Netherlands: two active custom-designed broadband UV-based miniDOAS (Differential Optical Absorption Spectroscopy) instruments and a commercially available infrared-based quantum cascade laser HT8700E gas analyser developed by the company Healthy Photon (HT). Both instruments avoid the hysteresis effects caused by the stickiness of NH_3 to tubing and instrument ~~interior~~interiors, and are as such insensitive to interference by ammonium aerosols. Both instruments showed good uptime during the campaign. The uptime of the miniDOAS system reached 100% once operational, but regular intercalibration of the two instruments was applied to test baseline stability (35% of the 7-week uptime). Intercalibration time can be reduced in future application based on the results of this campaign. The HT does not measure during rain, or shortly after rain while the instrument is drying. The coating of HT mirrors tended to degrade because of rain, causing 21% data loss during the 5-week uptime.

The miniDOAS system measured fluxes using the aerodynamic gradient method (AGM), the HT8700E measured fluxes using the eddy covariance (EC) method. After data quality filtering, a total of 848 simultaneous half-hourly flux measurements were compared, showing that both instruments gave similar values for the NH_3 exchange ranging from *ca.* -80 to 140 ng NH_3 m^{-2} s^{-1} (Figure 10). When the upwind terrain was both homogenous and free of nearby obstacles within around 100 m, the two systems showed the strongest correlation ($n = 113$, $r = 0.87$) and provided similar temporal patterns. In addition, the observed diurnal pattern of the two systems had the same shape (Figure 11). As such, the deposition flux during night-time was ca. 25 ng NH_3 m^{-2} s^{-1} (equivalent to 465 mol NH_3 ha^{-1} yr^{-1}). The highest emission occurred around noon and was up to 50 ng NH_3 m^{-2} s^{-1}. Moreover, the AGM flux values were larger than the EC ones during daytime.

The uncertainty analysis showed that the random error of the two systems was similar (Figure 12). The median relative random errors were 23% for the AGM flux versus 15% for the EC flux. The ~~mean~~median random error (1σ) for half-hourly flux values of the miniDOAS was about ~~9.8~~7.4 ng NH_3 m^{-2} s^{-1}, and its maximum value generally did not exceed 15 ng m^{-2} s^{-1}. For the HT, the ~~mean~~median and maximum random errors were ~~5.5~~4.1 and 10 ng NH_3 m^{-2} s^{-1}, respectively. These values are adequate to allow the study of deposition and emission processes. The random errors of both techniques varied substantially with meteorological conditions and time-of-day. For AGM flux, it was relatively higher during daytime. The diurnal cycle in the random error of the EC was, on the other hand, far less distinct.

While flux measurements between HT and miniDOAS in general compared well, we found a substantial variable offset in the HT concentrations. They were sensitive to air temperature, causing substantial differences (range: -15 to + 6 µg m^{-3}) between the two systems. In this study, we used the miniDOAS as a reference to correct the HT concentration using a temperature-dependent offset and assuming no impact on the span. It should be stressed that these offset corrections only have an impact

on the HT concentrations, not (or only very minor) on the HT fluxes. However, a temperature dependency in the span would also affect the HT fluxes. Further studies into the temperature dependence of the HT concentrations are needed to confirm the span calibration is indeed not impacted by changes in temperature.

The footprint analysis for the EC method showed that measurements were representative of the terrain up to approximately 100 m upwind. In the southeast direction, the footprint size was much smaller due to the meteorological measurement tower, which largely blocked the air flow. The footprint size of the AGM was not analysed but is expected to have a similar shape. Moreover, because of the lower measurement heights, the miniDOAS system is expected to have a smaller footprint, and the footprints of upper and lower paths are substantially different.

Spatial heterogeneous flux patterns need to be avoided in the upwind footprint region as they can influence the result and render interpretation more complicated or even impossible. Also, the 10% difference found between the theoretical (Moncrieff et al., 1997) and empirical (Wintjen et al., 2020) method for correcting high-frequency losses of EC fluxes may be related to inhomogeneities in the footprint area since they were not reproduced by theoretical cospectra. In addition, the terrain within all footprints needs to be homogeneous in its vegetation type and roughness. For further intercomparisons, obstacles-free, cattle-free, more homogeneous surroundings are highly recommended.

In deposition studies and parametrisations, reliable concentration and flux values are both needed. The miniDOAS provides both values reliably and appeared ready for long-term hands-off monitoring. The HT is presented solely as a flux instrument, and makes no claim to being an accurate monitor for NH_3 concentrations yet. In addition, the current system had a limited stand-alone operational time under the prevailing weather conditions.

In this study, we demonstrated that the miniDOAS and HT8700 systems provide comparable flux measurements at half-hourly time resolution. Under the right circumstances, data from both instruments can facilitate the study of processes behind dry deposition in different ecosystems, allowing better understanding and better parametrization of these processes in chemical transport models. These observations also enable to test and validate low-cost deposition measurement systems like the conditional time-averaged gradient (COTAG; Famulari et al., 2010), or inferential deposition networks (e.g. those listed by Walker et al., 2020).

7 Author contribution

DS, AH, SR and TvG designed the study. DS and AH coordinated the field campaign. DS, SB, RvdH and MH developed and tested the miniDOAS instruments and performed measurements during the campaign. JZ, AH, AF and PvdB performed the EC HT measurements. JZ and PW processed the EC and HT data and determined the EC NH_3 flux. SB processed miniDOAS concentration data, and SvdG determined the AGM NH_3 flux. Figures were made by SvdG, SB and JZ. DS, AH and SR prepared the manuscript with contributions from JZ, SvdG, and SB. MvZ, RS, PW and TvG reviewed and corrected the draft manuscript.

8 Competing interests

The authors declare that they have no conflict of interest.

9 Acknowledgements

This work was done partly in the framework of the Dutch Ruisdael program (https://ruisdael-observatory.nl) and was part of the annual Ruisdael campaign (RITA-2021). Funding from the Ministry of Agriculture, Nature and Food Quality (LNV) is gratefully acknowledged. We thank the Royal Netherlands Meteorological Institute (KNMI) for site access and assistance during the campaign, especially Arnoud Apituley for coordination and help with site selection. We thank Dr. Kai Wang, from Institute of Atmospheric Physics, Chinese Academy of Sciences, Beijing; and staff from Healthy Photon Lt. Co, especially Dr. Yin Wang and Dr. Peng Kang ~~are,~~ for helpful discussions about data processing of the HT. Furthermore, we thank Daniëlle van Dinther (TNO) for merging various data streams during the campaign. We acknowledge RIVM colleagues Kim Vendel for the preliminary processing of the AGM data at beginning of the campaign, and Miranda Braam for helping with the uncertainty analysis.

10 References

Bai, M., Suter, H., Macdonald, B., and Schwenke, G.: Ammonia, methane and nitrous oxide emissions from furrow irrigated cotton crops from two nitrogen fertilisers and application methods, Agricultural and Forest Meteorology, 303, 108375, https://doi.org/10.1016/j.agrformet.2021.108375, 2021.

Bai, M., Loh, Z., Griffith, D. W. T., Turner, D., Eckard, R., Edis, R., Denmead, O. T., Bryant, G. W., Paton-Walsh, C., Tonini, M., McGinn, S. M., and Chen, D.: Performance of open-path lasers and FTIR spectroscopic systems in agriculture emissions research, Atmos. Meas. Tech. Discuss., 2022, 1-18, 10.5194/amt-2021-347, 2022.

Beljaars, A. C. M. and Holtslag, A. A. M.: Flux parameterization over land surfaces for atmospheric models, Journal of Applied Meteorology, 30, 327-341, https://www.doi.org/10.1175/1520-0450(1991)030<0327:Fpolsf>2.0.Co;2, 1991.

Berkhout, A. J. C., Swart, D. P. J., Volten, H., Gast, L. F. L., Haaima, M., Verboom, H., Stefess, G., Hafkenscheid, T., and Hoogerbrugge, R.: Replacing the AMOR with the miniDOAS in the ammonia monitoring network in the Netherlands, Atmospheric Measurement Techniques, 10, 4099-4120, 10.5194/amt-10-4099-2017, 2017.

Bosveld, F. C.: The Cabauw in-situ observational program 2000 - present: instruments, calibrations and set-up, Royal Netherlands Meteorological Institute, De Bilt, 2020.

Bosveld, F. C., Baas, P., Beljaars, A. C. M., Holtslag, A. A. M., de Arellano, J. V.-G., and van de Wiel, B. J. H.: Fifty years of atmospheric boundary-layer research at Cabauw serving weather, air quality and climate, Boundary-Layer Meteorology, 177, 583-612, 10.1007/s10546-020-00541-w, 2020.

Burba, G., Anderson, T., and Komissarov, A.: Accounting for spectroscopic effects in laser-based open-path eddy covariance flux measurements, Global Change Biology, 25, 2189-2202, https://doi.org/10.1111/gcb.14614, 2019.

Businger, J. A.: Evaluation of the accuracy with which dry deposition can be measured with current micrometeorological techniques, Journal of Climate and Applied Meteorology, 25, 1100-1124, 1986.

Dyer, A. J.: A review of flux-profile relationships, Boundary-Layer Meteorology, 7, 363-372, https://www.doi.org/10.1007/BF00240838, 1974.

Erisman, J. W. and Wyers, G. P.: Continuous measurements of surface exchange of SO_2 and NH_3; Implications for their possible interaction in the deposition process, Atmospheric Environment. Part A. General Topics, 27, 1937-1949, https://doi.org/10.1016/0960-1686(93)90266-2, 1993.

Erisman, J. W., Galloway, J. N., Dice, N. B., Sutton, M. A., Bleeker, A., Grizzetti, B., Leach, A. M., and Vries, W. d.: Nitrogen: too much of a vital resource, Science Brief. WWF Netherlands, Zeist, The Netherlands, 2015.

Famulari, D., Fowler, D., Hargreaves, K., Milford, C., Nemitz, E., Sutton, M. A., and Weston, K.: Measuring eddy covariance fluxes of ammonia using tunable diode laser absorption spectroscopy, J Water, Air, Soil Pollution: Focus, 4, 151-158, 10.1007/s11267-005-3025-9, 2004.

Famulari, D., Fowler, D., Nemitz, E., Hargreaves, K. J., Storeton-West, R. L., Rutherford, G., Tang, Y. S., Sutton, M. A., and Weston, K. J.: Development of a low-cost system for measuring conditional time-averaged gradients of SO_2 and NH_3, Environmental Monitoring Assessment, 161, 11-27, 10.1007/s10661-008-0723-6, 2010.

Flechard, C. R., Nemitz, E., Smith, R. I., Fowler, D., Vermeulen, A. T., Bleeker, A., Erisman, J. W., Simpson, D., Zhang, L., Tang, Y. S., and Sutton, M. A.: Dry deposition of reactive nitrogen to European ecosystems: a comparison of inferential models across the NitroEurope network, Atmospheric Chemistry and Physics, 11, 2703-2728, https://www.doi.org/10.5194/acp-11-2703-2011, 2011.

Flesch, T. K., Baron, V. S., Wilson, J. D., Griffith, D. W. T., Basarab, J. A., and Carlson, P. J.: Agricultural gas emissions during the spring thaw: Applying a new measurement technique, Agricultural and Forest Meteorology, 221, 111-121, https://doi.org/10.1016/j.agrformet.2016.02.010, 2016.

Foken, T.: Micrometeorology, 2017.

Fowler, D., Coyle, M., Skiba, U., Sutton, M. A., Cape, J. N., Reis, S., Sheppard, L. J., Jenkins, A., Grizzetti, B., Galloway, J. N., Vitousek, P., Leach, A., Bouwman, A. F., Butterbach-Bahl, K., Dentener, F., Stevenson, D., Amann, M., and Voss, M.: The global nitrogen cycle in the twenty-first century, Philosophical Transactions of the Royal Society B: Biological Sciences, 368, 20130164, 10.1098/rstb.2013.0164, 2013.

Galloway, J. N., Bleeker, A., and Erisman, J. W.: The human creation and use of reactive nitrogen: a global and regional perspective, Annual Review of Environment and Resources, 46, 255-288, 10.1146/annurev-environ-012420-045120, 2021.
Homan, C.: Maandoverzichtt van het weer in Nederland, September 2021, KNMI, De Bilt, 2021.
Hoogerbrugge, R., Geilenkirchen, G. P., Hollander, H. A. d., Schuch, W., Swaluw, E. v. d., Vries, W. J. d., and Kruit, R. J. W.: Grootschalige concentratie- en depositiekaarten Nederland - Rapportage 2020, Rijksinstituut voor Volksgezondheid en Milieu, Bilthoven, 2020.
Horst, T. W., Vogt, R., and Oncley, S. P.: Measurements of flow distortion within the IRGASON integrated sonic anemometer and CO_2/H_2O gas analyzer, Boundary-Layer Meteorology, 160, 1-15, 10.1007/s10546-015-0123-8, 2016.
Jager, C. J., Nakken, T. C., and Palland, C. L.: Bodemkundig onderzoek van twee graslandpercelen nabij Cabauw. , Arnhem (In Dutch), 1976.
Kaimal, J. C., Wyngaard, J. C., Izumi, Y., and Coté, O. R.: Spectral characteristics of surface-layer turbulence, Quarterly Journal of the Royal Meteorological Society, 98, 563-589, https://doi.org/10.1002/qj.49709841707, 1972.
Kamp, J. N., Häni, C., Nyord, T., Feilberg, A., and Sørensen, L. L.: The aerodynamic gradient method: implications of non-simultaneous measurements at alternating heights, Atmosphere, 11, 1067, 2020.
Kljun, N., Calanca, P., Rotach, M. W., and Schmid, H. P.: A simple two-dimensional parameterisation for Flux Footprint Prediction (FFP), Geosci. Model Dev., 8, 3695-3713, 10.5194/gmd-8-3695-2015, 2015.
Loubet, B. and Personne, E.: Application note 28 - Measuring emissions from diffuse sources using the aerodynamic gradient, in: Measuring emissions from livestock farming: greenhouse gases, ammonia and nitrogen oxides, edited by: Hassouna, M., Eglin, T., Cellier, P., Colomb, V., Cohan, J.-P., Decuq, C., Delabuis, M., Edouard, N., Espagnol, S., Eugène, M., Fauvel, Y., Fernandes, E., Fischer, N., Flechard, C., Genermont, S., Godbout, S., Guingand, N., Guyader, J., Lagadec, S., Laville, P., Lorinquer, E., Loubet, B., Loyon, L., Martin, C., Méda, B., Morvan, T., Oster, D., Oudart, D., Personne, E., Planchais, J., Ponchant, P., Renand, G., Robin, P., and Rochette, Y., INRA-ADEME, np, 2016.
Loubet, B., Decuq, C., Personne, E., Massad, R. S., Flechard, C., Fanucci, O., Mascher, N., Gueudet, J. C., Masson, S., Durand, B., Genermont, S., Fauvel, Y., and Cellier, P.: Investigating the stomatal, cuticular and soil ammonia fluxes over a growing tritical crop under high acidic loads, Biogeosciences, 9, 1537-1552, 10.5194/bg-9-1537-2012, 2012.
Loubet, B., Cellier, P., Fléchard, C., Zurfluh, O., Irvine, M., Lamaud, E., Stella, P., Roche, R., Durand, B., Flura, D., Masson, S., Laville, P., Garrigou, D., Personne, E., Chelle, M., and Castell, J.-F.: Investigating discrepancies in heat, CO2 fluxes and O3 deposition velocity over maize as measured by the eddy-covariance and the aerodynamic gradient methods, Agricultural and Forest Meteorology, 169, 35-50, https://doi.org/10.1016/j.agrformet.2012.09.010, 2013.
Mauder, M. and Foken, T.: Impact of post-field data processing on eddy covariance flux estimates and energy balance closure Meteorologische Zeitschrift, 15, 597-609, https://doi.org/10.1127/0941-2948/2006/0167, 2006.
Mauder, M., Foken, T., Aubinet, M., and Ibrom, A.: Eddy-covariance measurements, in: Springer Handbook of Atmospheric Measurements, edited by: Foken, T., Springer International Publishing, Cham, 1485-1515, 10.1007/978-3-030-52171-4_55, 2021.
McDermitt, D. K., Burba, G., Xu, L., Anderson, T. G., Komissarov, A. V., Riensche, B., Schedlbauer, J. L., Starr, G., Zona, D., Oechel, W. C., Oberbauer, S. F., and Hastings, S. J.: A new low-power, open-path instrument for measuring methane flux by eddy covariance, Applied Physics B, 102, 391-405, doi:10.1007/s00340-010-4307-0, 2011.
Miller, D. J., Sun, K., Tao, L., Khan, M. A., and Zondlo, M. A.: Open-path, quantum cascade-laser-based sensor for high-resolution atmospheric ammonia measurements, Atmos. Meas. Tech., 7, 81-93, 10.5194/amt-7-81-2014, 2014.
Moncrieff, J., Clement, R., Finnigan, J., Meyers, T., Lee, X., Massman, W., and Law, B.: Averaging, detrending, and filtering of eddy covariance time series, in: Handbook of micrometeorology; A guide for surface flux measurement and analysis, edited by: Lee, X., Massman, W., and Law, B., Atmospheric and oceanographic sciences library, Kluwer Academic Publisher, Dordrecht, The Netherlands, 7-32, 2004.
Moncrieff, J. B., Massheder, J. M., de Bruin, H., Elbers, J., Friborg, T., Heusinkveld, B., Kabat, P., Scott, S., Soegaard, H., and Verhoef, A.: A system to measure surface fluxes of momentum, sensible heat, water vapour and carbon dioxide, Journal of Hydrology, 188-189, 589-611, https://doi.org/10.1016/S0022-1694(96)03194-0, 1997.
Moore, C. J.: Frequency response corrections for eddy correlation systems, Boundary-Layer Meteorology, 37, 17-35, 10.1007/BF00122754, 1986.
Moravek, A., Singh, S., Pattey, E., Pelletier, L., and Murphy, J. G.: Measurements and quality control of ammonia eddy covariance fluxes: a new strategy for high-frequency attenuation correction, Atmos. Meas. Tech., 12, 6059-6078, 10.5194/amt-12-6059-2019, 2019.
Pan, D., Benedict, K. B., Golston, L. M., Wang, R., Collett, J. L., Tao, L., Sun, K., Guo, X., Ham, J., Prenni, A. J., Schichtel, B. A., Mikoviny, T., Müller, M., Wisthaler, A., and Zondlo, M. A.: Ammonia dry deposition in an alpine ecosystem traced to agricultural emission hotpots, Environmental Science & Technology, 55, 7776-7785, 10.1021/acs.est.0c05749, 2021.
Parrish, D. D. and Fehsenfeld, F. C.: Methods for gas-phase measurements of ozone, ozone precursors and aerosol precursors, Atmospheric Environment, 34, 1921-1957, https://doi.org/10.1016/S1352-2310(99)00454-9, 2000.
Paulson, C. A.: The mathematical representation of wind speed and temperature profiles in the unstable atmospheric surface layer, Journal of Applied Meteorology, 9, 857-861, https://www.doi.org/10.1175/1520-0450(1970)009<0857:Tmrows>2.0.Co;2, 1970.
Platt, U. and Stutz, J.: Differential Optical Absorption Spectroscopy - Principles and Applications, Springer, Berlin2008.
Prueger, J. H. and Kustas, W. P.: Aerodynamic methods for estimating turbulent fluxes in: Micrometeorology in Agricultural Systems, American Society of Agronomy, Crop Science Society of America, Soil Science Society of America, Madison, 2005.

Schulte, R. B., van Zanten, M. C., Rutledge-Jonker, S., Swart, D. P. J., Wichink Kruit, R. J., Krol, M. C., van Pul, W. A. J., and Vilà-Guerau de Arellano, J.: Unraveling the diurnal atmospheric ammonia budget of a prototypical convective boundary layer, Atmospheric Environment, 118153, https://doi.org/10.1016/j.atmosenv.2020.118153, 2020.
Sintermann, J., Dietrich, K., Häni, C., Bell, M., Jocher, M., and Neftel, A.: A miniDOAS instrument optimised for ammonia field measurements, Atmospheric Measurement Techniques, 9, 2721-2734, 10.5194/amt-9-2721-2016, 2016.
Sintermann, J., Ammann, C., Kuhn, U., Spirig, C., Hirschberger, R., G¨artner, A., and Neftel, A.: Determination of field scale ammonia emissions for common slurry spreading practice with two independent methods, Atmospheric Measurement Techniques, 4, 1821-1840, 2011.
Sun, K., Tao, L., Miller, D. J., Zondlo, M. A., Shonkwiler, K. B., Nash, C., and Ham, J. M.: Open-path eddy covariance measurements of ammonia fluxes from a beef cattle feedlot, Agricultural and Forest Meteorology, 213, 193-202, http://dx.doi.org/10.1016/j.agrformet.2015.06.007, 2015.
Sutton, M. A., Oenema, O., Erisman, J. W., Leip, A., van Grinsven, H., and Winiwarter, W.: Too much of a good thing, Nature, 472, 159-161, 10.1038/472159a, 2011.
Trebs, I., Ammann, C., and Junk, J.: Immission and dry deposition, in: Springer Handbook of Atmospheric Measurements, edited by: Foken, T., Springer Handbooks, Springer, Cham., https://doi.org/10.1007/978-3-030-52171-4_54, 2021.
Volten, H., Haaima, M., Swart, D., van Zanten, M., and van Pul, W.: Ammonia exchange measured over a corn field in 2010, National Institute of Public Health and the Environment, Bilthoven, The Netherlands, 2012a.
Volten, H., Bergwerff, J. B., Haaima, M., Lolkema, D. E., Berkhout, A. J. C., van der Hoff, G. R., Potma, C. J. M., Wichink Kruit, R. J., van Pul, W. A. J., and Swart, D. P. J.: Two instruments based on differential optical absorption spectroscopy (DOAS) to measure accurate ammonia concentrations in the atmosphere, Atmospheric Measurement Techniques, 5, 413-427, https://www.doi.org/10.5194/amt-5-413-2012, 2012b.
Walker, J. T., Beachley, G., Zhang, L., Benedict, K. B., Sive, B. C., and Schwede, D. B.: A review of measurements of air-surface exchange of reactive nitrogen in natural ecosystems across North America, Science of The Total Environment, 698, 133975, https://doi.org/10.1016/j.scitotenv.2019.133975, 2020.
Walker, J. T., Jones, M. R., Bash, J. O., Myles, L., Meyers, T., Schwede, D., Herrick, J., Nemitz, E., and Robarge, W.: Processes of ammonia air–surface exchange in a fertilized *Zea mays* canopy, Biogeosciences, 10, 981-998, 10.5194/bg-10-981-2013, 2013.
Wang, K., Kang, P., Lu, Y., Zheng, X., Liu, M., Lin, T.-J., Butterbach-Bahl, K., and Wang, Y.: An open-path ammonia analyzer for eddy covariance flux measurement, Agricultural and Forest Meteorology, 308-309, 108570, https://doi.org/10.1016/j.agrformet.2021.108570, 2021.
Wang, K., Wang, J., Qu, Z., Xu, W., Wang, K., Zhang, H., Shen, J., Kang, P., Zhen, X., Wang, Y., Zheng, X., and Liu, X.: A significant diurnal pattern of ammonia dry deposition to a cropland is detected by an open-path quantum cascade laser-based eddy covariance instrument, Atmospheric Environment, https://doi.org/10.1016/j.atmosenv.2022.119070, 2022.
Webb, E. K., Pearman, G. I., and Leuning, R.: Correction of flux measurements for density effects due to heat and water vapour transfer, Quarterly Journal of the Royal Meteorological Society, 106, 85-100, https://doi.org/10.1002/qj.49710644707, 1980.
Wichink Kruit, R. J., H, V., M, H., DPJ, S., MC, v. Z., and WAJ, v. P.: Ammonia exchange measurements over a corn field in Lelystad, the Netherlands in 2009, National Institute for Public Health and the Environment, Bilthoven, The Netherlands, 2010.
Wintjen, P., Ammann, C., Schrader, F., and Brümmer, C.: Correcting high-frequency losses of reactive nitrogen flux measurements, Atmos. Meas. Tech., 13, 2923-2948, 10.5194/amt-13-2923-2020, 2020.
Wolff, V., Trebs, I., Ammann, C., and Meixner, F. X.: Aerodynamic gradient measurements of the NH_3-HNO_3-$NH4NO_3$ triad using a wet chemical instrument: an analysis of precision requirements and flux errors, Atmos. Meas. Tech., 3, 187-208, https://www.doi.org/10.5194/amt-3-187-2010, 2010.
Zöll, U., Brümmer, C., Schrader, F., Ammann, C., Ibrom, A., Flechard, C. R., Nelson, D. D., Zahniser, M., and Kutsch, W. L.: Surface–atmosphere exchange of ammonia over peatland using QCL-based eddy-covariance measurements and inferential modeling, Atmospheric Chemistry and Physics, 16, 11283-11299, 10.5194/acp-16-11283-2016, 2016.